Exploring Mechanisms of Early Acquired Resistance to Doxorubicin in Melanoma in 3D Model

Abstract

Chemoresistance continues to remain a significant barrier to the effective treatment of various cancers, including melanoma. Previous studies, including our own, have demonstrated the limited efficacy of doxorubicin (DOX) against melanoma cells and tumors, both in vitro and in vivo, primarily due to acquired chemoresistance. Furthermore, the lack of favorable outcomes for patients with metastatic melanoma treated with liposomal DOX underscores the urgent need for identifying early biomarkers of DOX-induced chemoresistance and develop combination strategies to improve its therapeutic efficacy and overcome drug resistance. This study examines early adaptive responses in B16.F10 melanoma cells grown as spheroids, after two exposures to DOX used at sub-inhibitory concentration ($\approx IC_{30}$). The investigated processes associated with early establishment of chemoresistance involved cycle regulation, DNA damage and repair mechanisms, apoptosis, angiogenesis, and dissemination potential. Melanoma spheroids were cultured in ultra-low attachment plates and treated with DOX in two 48-hour phases separated by 48-hour recovery periods, followed by viability, morphology, gene/protein expression, and enzyme activity assessments using RNA-seq, RT-qPCR, Western blot, and gelatinase assay, respectively. Functional analysis confirmed downregulation of cell cycle pathways, suppression of stress response and survival pathways (e.g., TNFA_SIGNALING_VIA_NFKB and MTORC1_SIGNALING). Despite mRNA data showing cell cycle arrest (downregulated *CDK1, Ticrr, Cdc20*) and major DNA damage and impaired repair (downregulated *BRIP1, BARD1, Rad51, Rmi2*), after first exposure to DOX, cells probably bypassed cell cycle checkpoints by upregulating transcripts and proteins linked to pro-survival (*Tnfrsf19*, cIAP-2) and angiogenesis (VEGF, eotaxin-1), and by upregulating transcripts related to cell adhesion (*Pcdh beta* family members), and ECM remodeling (*Ecm1*, *Jam2*), suggesting early adaptation mechanisms to DOX. With a second DOX exposure, melanoma spheroids showed stronger chemoresistance, evidenced by enhanced angiogenesis (upregulated *Aqp1, VEGF,* and *Ackr3*), increased invasiveness (upregulated *MMP-2*, favored MMP-9 activity), and a 40% increase in pNF-kB levels, reinforcing drug tolerance and aggressiveness. This study provides valuable insights into the molecular drivers of chemoresistance, revealing that early DOX resistance in melanoma arises from adaptive mechanisms enhancing survival, angiogenesis, and invasiveness. Repeated exposure to DOX reinforces these traits, sustaining drug tolerance.

Funding and acknowledgments

This work was supported by L'Oréal - UNESCO “For Women in Science" [Fellowship Programme no. 914, 2020]; the UEFISCDI grant [PN-III-P2-2_1-PED-2021-0411, No. 659PED, 2022] granted to dr. Alina Sesarman.

Keywords: 3D melanoma model, early acquired resistance, doxorubicin, sub-inhibitory concentration, tumor progression mechanisms

Introduction

Despite significant advancements in anticancer therapies over recent decades, the development of cancer cell resistance to cytostatic drugs, including doxorubicin (DOX), remains a major obstacle for effective treatments, especially in cancers like skin melanoma, breast, ovarian, and liver (Amaral et al., 2019; N.-N. Chen et al., 2023; Q. Chen & Wang, 2020; Christowitz et al., 2019; Cox & Weinman, 2016; Elliott & Al-Hajj, 2009; Januchowski et al., 2016; Khan et al., 2024; Licarete et al., 2020; Lovitt et al., 2018; McDermott et al., 2014; Rezayatmand et al., 2022; L. Smith et al., 2006) . Previous studies, including ours, have established the poor efficacy of DOX on melanoma cells or against melanoma tumors, *in vivo* (Elliott & Al-Hajj, 2009; Licarete et al., 2020; Panneerselvam et al., 1987) due to acquired chemoresistance. Moreover, the lack of a successful response in clinical studies of liposomal DOX, on human metastatic melanoma (Vorobiof et al., 2003) emphasizes the need for combination or other innovative approaches to enhance therapeutic outcomes, and overcome drug-resistance (Licarete et al., 2019; Negrea et al., 2022). Traditional 2D cell cultures are valuable tools in cancer research but often fail to replicate the complexity of *in vivo* tumors, leading to discrepancies in gene/protein expression and treatment responses (Kapałczyńska et al., 2016) . In contrast, 3D cell culture models better simulate the tumor architecture by promoting realistic cell-cell and cell-matrix interactions. As a result, gene expression in 3D cultures more closely resembles clinical tumors, making them a more reliable platform for studying drug responses and tumor behavior (Pampaloni et al., 2007). This study investigated the early mechanisms of DOX resistance in B16.F10 melanoma cells following repeated exposure to a sub-inhibitory concentration (≈IC30). Using a 3D spheroid model in a commercial ECM (1.5%), we mimicked conditions that enrich quiescent cancer stem cells, known to drive therapy resistance (Amaral et al., 2019; Filipiak-Duliban et al., 2022; McDermott et al., 2014). The experimental setup involved cyclic DOX treatments with a 48-hour recovery phase between exposures to assess both immediate and adaptive responses following DOX exposure. Spheroids viability was assessed throughout the experiment using an acid phosphatase viability assay. Gene expression changes were analyzed using RNA-seq and RT-qPCR, while protein and enzyme activities were assayed by western blot, protein array and gelatinase assays. Thus, alteration in key processes associated with chemoresistance were investigated, with a focus on key pathways such as cell cycle regulation, DNA damage and repair, apoptosis, angiogenesis and migration (or invasion/metastasis). Our findings indicate that melanoma cells in our 3D model showed early signs of DOX-induced resistance, adapting to sub-inhibitory DOX treatment by altering key molecular pathways, promoting tumor progression and therapy resistance. DOX-induced resistance involved cell cycle arrest (*CDK1, Cyclin G1, Ticrr, Cdc20, Bub1*), impaired DNA repair (*BRIP1, BARD1, Rad51, Rmi2*), and activation of escape mechanisms driving angiogenesis (*VEGF, MMP-2, Aqp1, Ackr3*) and migration (*MMP-2, MMP-9*). Upon re-exposure to DOX, these pathways were further enhanced alongside pro-survival mechanisms (*decreased Cyclin G1, Sfn*), leading to a more aggressive, NF-kB-driven phenotype. Together, our results underscore the importance of identifying early signs of drug-resistance in order to simultaneously target cell proliferation, DNA damage tolerance, apoptotic resistance and aggressiveness pathways, to overcome therapy evasion in melanoma. Further studies should explore the impact of cyclic DOX treatments and their long-term effects in a more complex TME model.

Materials and Methods

Murine Melanoma Spheroids Formation and Growth

For spheroid formation using liquid-overlayer technique 5x10^3 B16.F10 cells/well (ATCC; CRL-6457, Lonza Group, Basel, Switzerland CH) were seeded in ultra-low attachment 96-well plate, using standard DMEM medium, supplemented with 10% FCS, Pen/Strep and L-Glutamine, 4.5 g/l glucose) (Al-Hity et al., 2021; Carlsson & Yuhas, 1984; Metzger et al., 2011). To better replicate the tumor microenvironment (TME), melanoma cells were cultured as spheroids in non-adherent plates, embedded in commercial/artificial extracellular matrix (ECM) (Gonzalez-Fernandez et al., 2022). An 1.5% ECM gel (Sigma-Aldrich E1270) was incorporated into each well according to established protocols to support spheroid formation in an ECM-enriched environment (Ahmad et al., 2017; Costa et al., 2014). The plates were centrifuged for 15 min at 350 x g, then placed in a 37°C humidified incubator with 5% CO_2 until round-shaped spheroids were formed. This method allowed the formation of three-dimensional (3D) structures that closely mimic cell-cell and cell-matrix interactions that contribute to drug resistance. After 4 days of incubation, spheroids of 400–500 μm diameter were obtained. Images of spheroids were taken daily using Zeiss Axio Vert.A1 inverted microscope (ZEISS), with a 5x objective (magnification 50x), and an high-throughput image analysis software application - SpheroidSizer (https://bit.ly/4hQBJZf), in order to measure their diameter and volume (W. Chen et al., 2014).

Viability assay

To assess cell viability within the spheroids, a modified version of the acid phosphatase (APH) assay was performed (Friedrich et al., 2007). Active acid phosphatases catalyze the hydrolysis of p-nitrophenyl phosphate, generating p-nitrophenol in viable cells. 100 μL of the assay buffer containing 0.2M acetate buffer 5.8pH, 0.1% Triton X-100 and 2mg/ml p-nitrophenyl phosphate was added per well and incubated for 30 min at 37°C. After incubation, the enzymatic reaction was stopped by adding 10 μL of 1 M NaOH to each well, and the absorbance at 405 nm was measured within 10 minutes using a microplate reader (FLUOstar Omega, BMG, Labtech, Offenburg, Germany). Cell viability within spheroids was expressed as a percentage from the viability of cells in control (untreated) spheroids. All experiments were conducted in triplicate. All data were expressed as the mean ± standard deviation (SD) (n=9).

Drug treatment

DOX was purchased from Sigma-Aldrich (Chemie GmbH, Germany). On day 4 of spheroid growth, DOX solutions of increasing concentration (ranging from 0.156 µM -10 µM) were applied onto the spheroids. Untreated spheroids were used as control. Drug effects on B16.F10 melanoma cells grown as spheroids were determined after 48 hrs of treatment by measuring cell viability (using APH assay) and spheroid volume (Friedrich et al., 2007) . Based on APH viability assay results, the IC50 value of DOX was determined (**Figure 1A**), as well as it's corresponding to sub-inhibitory IC30 value, which was used for the cyclic exposure of spheroids to DOX and found to be 0.282 µM. Further, the spheroids were subjected to two exposures to DOX at this IC30 concentration (0.282 µM), separated by a 48-hour recovery phase, as represented in **Figure 1B**, to simulate repeated drug exposure found in clinical settings (Fey et al., 2020a; Kuczynski et al., 2013) . **Figure 1B** also shows representative images of spheroids throughout the entire experiment (day 1-day 10). On day 6, 48 hours after receiving the first DOX treatment, a subset of spheroids was collected, washed with PBS, and processed for RNA, DNA and protein extraction, alongside the control group (CTR1), while the remaining subset of DOX-treated spheroids was used for further experiments. Precisely, to further determine the effects of a second exposure to DOX, spheroids initially treated with DOX were collected, washed with PBS, disintegrated with trypsin, centrifuged 15 min at 350xg, and the remaining cells were cultured for 48 hrs in ECM-enriched DMEM medium (recovery phase), to allow for spheroid reassembly. Reformed spheroids were re-exposed to DOX (0.282 µM) for 48 hrs (DOX2), while reformed untreated spheroids were used as control (CTR2). Each treatment phase began with drug administration, lasting 48 hours before drug removal, while recovery phase followed the same timing with addition and removal of culture medium (Lamichhane et al., 2022; Lamichhane & Tavana, 2024) . 48 hrs after the second exposure to DOX (IC30), cell viability was assessed by APH assay (**Figure 2A**). Additionally, total RNA and proteins were extracted from the spheroids exposed to DOX and control spheroids, to analyze gene and protein expression levels associated with drug resistance mechanisms. Average growth rates (k_{DOX}, k_{CTR}) of melanoma spheroids during the two exposures to DOX treatment were calculated (k_{DOX}) compared to growth rates of controls spheroids (k_{CTR}) and expressed as mean ±SD (**Figure 2B,C**). k_{DOX}/k_{CTR} ratio resistance growth was also calculated and served as a metric for quantifying resistance to DOX treatment (Shahi Thakuri et al., 2019) (**Figure 2B,C**). A k_{DOX}/k_{CTR} ratio ≥ 1, indicates resistance to DOX treatment, while a ratio < 1 suggests DOX-induced growth inhibition (sensitivity to DOX) (Shahi Thakuri et al., 2019). The growth rate for treated spheroids (k_{DOX}) was calculated as the change in spheroids volume between the end and beginning of each phase. The control growth rate (k_{CTR}) was calculated as the change in volume of control (untreated) spheroids over the same period. k_{DOX}/k_{CTR} normalized growth rate was calculated as the ratio between the growth rate of DOX-treated spheroids (k_{DOX}) and the growth rate of control (untreated) spheroids (k_{CTR}).

RNA isolation for RNA-sequencing

48 hours after the initial DOX exposure, treated and control spheroids were collected, washed with PBS, and processed for total RNA using RNeasy Mini Kit (Qiagen, 74104) according to the manufacturer's instructions (Longati et al., 2013). The RNA was eluted with 40 µl of RNase-free water. RNA quality/integrity was determined using NanoDrop 1000 (Thermo Scientific, Ma, USA) according to the manufacturer's protocol (Zhang et al., 2020). To generate strand-specific cDNA libraries, TruSeq Stranded mRNA Library Prep Kit (Illumina, Inc.) was used, followed by quality control procedure. The qualified libraries were then subjected to sequencing by Illumina platform, Paired-ends 101 (Illumina, Inc.). Two biological replicates were used for each experimental group (Q. Wang et al., 2017). Library construction and sequencing were performed by Macrogen Europe (https://www.macrogen-europe.com/).

RNA-sequencing data analysis

The trimmed reads were mapped to the mouse reference genome using HISAT2 (v2.0.5). Transcript assembly was performed with StringTie-eB (v1.3.1), and the abundance of transcript was reported as read counts and normalized values (FPKM, CPM, TPM) (Pertea et al., 2015). The read count data were further preprocessed by filtering low quality transcripts and normalizing them with TMM method in the edgeR package. The differential expression was assessed using exactTest from edgeR (Pertea et al., 2016; Robinson et al., 2010), and the p-values were adjusted for multiple testing with Benjamini-Hochberg method (Benjamini et al., 2001; Benjamini & Yekutieli, 2001). The expression level of each gene in the spheroids receiving one single DOX treatment (DOX1) compared to the control group (CTR1) was calculated and expressed as fold regulation (FR) value. Genes with a FR cutoff of ± 2, a false discovery rate (FDR) less than 20% and a p-value less than 0.05 were considered differentially expressed. For differentially expressed genes (DEGs), we performed gene ontology (GO) enrichment analysis according to molecular function (MF), cellular component (CC), and biological process (BP) in g:Profiler (https://biit.cs.ut.ee/gprofiler/orth) (Kolberg et al., 2023; Raudvere et al., 2019; J. C. Smith & Sheltzer, 2022) and KEGG pathway annotation in the DAVID online tool (v2023q4), with significance thresholds set at FDR q-value $< 20\%$ and p-value < 0.05. The results from g:Profiler and DAVID were imported into R for visualization using the ggplot2 package. Additionally, volcano plots of all and of selected DEGs were generated in R utilizing the ggplot2 library (D. W. Huang et al., 2009; Sherman et al., 2022). Hierarchical clustering of the expression Z-scores of DEGs considered of interest (involved in the following processes: cell cycle, DNA damage and repair, apoptosis, angiogenesis, migration) was performed using R soft heatmap.2 function. For each row (each DEG) Z-scores were calculated as follows: $z=(x-\mu)/\sigma$, where x is the count value of the gene in a replicate, μ the mean of all count values of this gene in all replicates, and σ the corresponding SD (Weinguny et al., 2020). Gene Set Enrichment Analysis (GSEA) was performed in GSEA software to identify enriched signaling pathways between spheroids receiving one single DOX treatment (DOX1) compared to control spheroids (CTR1) using HALLMARK_database of gene expression data (Mootha et al., 2003; Subramanian et al., 2005). The analysis was conducted using the HALLMARK database of gene expression data, with significance thresholds set at FDR q-value < 20% and p-value < 0.05 to determine significantly enriched gene sets (Subramanian et al., 2005).

Quantitative Real-Time PCR (RT-qPCR)

RT-qPCR was conducted to confirm RNA-seq findings. 1 µg of total RNA was reverse transcribed into cDNA using iScript™ Reverse Transcription Supermix (#1708841, Bio-Rad Laboratories, Gladesville, Australia) in a 20 µL reaction volume, following manufacturer's instructions (Pflug et al., 2023) . The reaction mix was incubated at 25°C for 5 minutes for priming, followed by reverse transcription at 46°C for 20 minutes, and enzyme inactivation at 95°C for 1 minute. Real-time quantitative PCR was then performed with SsoFast™ EvaGreen® Supermix (#172-5200, Bio-Rad Laboratories, Gladesville, Australia). Each 1 µL cDNA sample was amplified with 500 nM of specific primers. The sequences (purchased from Eurogentec, Seraing, Belgium) are available in **Supplementary Table 1** (Negrea et al., 2025) (purchased from Eurogentec, Seraing, Belgium). The following setup was used for the amplification: enzyme activation at 95°C for 30 seconds, 40 cycles of denaturation at 95°C for 5 seconds, annealing at 55°C for 5 seconds, followed by a melting curve from 65°C to 95°C in 0.5°C increments. All reactions were run on the CFX96™ Real-Time System (C1000 Touch Thermal Cycler, Bio-Rad Laboratories, Gladesville, Australia) as per the manufacturer's protocol. Relative mRNA levels were calculated using the ΔΔCt method, with β-actin mRNA and ribosomal protein lateral stalk subunit P0 (Rplp0) serving as the internal references (Livak & Schmittgen, 2001).

Spheroids lysates preparation

After harvesting the B16.F10 spheroids, they were washed with PBS and lysed in 250 µl of radio-immunoprecipitation assay (RIPA) buffer (Invitrogen) containing proteases and phosphatases inhibitors (Invitrogen) (Filipiak-Duliban et al., 2022). Lysates were kept on ice for 30 minutes, followed by centrifugation at 4°C at 12 000 x *g* for 10 minutes. The supernatants were collected and stored at -80°C before further measurements (Luput et al., 2018). The total protein concentration of the cell lysates was determined using Bradford assay (Sigma-Aldrich; Merck KGaA) (Bradford, 1976; Rauca et al., 2018).

Western blot analysis

To determine the level of expression of pNF-kB in spheroid lysates, 50 µg of total protein *per* group were loaded onto a 10% polyacrylamide gel, followed by protein transfer to nitrocellulose membranes (Rauca et al., 2018). After blocking with 5% skimmed milk in TBS-T for 2 hours at room temperature, the membranes were incubated overnight at 4 °C with rabbit anti-mouse monoclonal antibody against mouse pNF-kB (1:1000) (sc-166748; A-8) and with rabbit anti-mouse antibody against mouse β-actin, respectively (1:1000) (A2103). Mouse β-actin was used as a loading control. The next day, the membranes were incubated with a goat anti-mouse HRP-conjugated secondary antibody (1:2500) (sc-2005) for 1 hour at room temperature. Washes with TBS-T were performed after every incubation step (Rauca et al., 2018). Immune complexes were detected using chemiluminescence and protein expression levels were quantified by densitometry using Image Lab Software 4.1 (Bio-Rad). Data from three independent experiments are presented as mean ± SD.

Angiogenesis array

To evaluate the impact of DOX treatment on the expression of angiogenic and inflammatory proteins in B16.F10 melanoma spheroids, a screening for 24 proteins involved in in these processes was performed, according to the manufacturer's protocol and as previously described in detail (Licarete et al., 2020) , using RayBio Mouse Angiogenic protein Antibody Array membranes 1.1 (RayBiotech Inc., Peachtree Corners, GA, USA). Briefly, the membranes were incubated overnight at 4°C with 250 µg of proteins from spheroids lysates, then with a primary biotinylated antibody cocktail specific for the 24 angiogenic/inflammatory proteins (diluted 1:1000) for 2 hrs, followed by a 2 hrs incubation with HRP-streptavidin at room temperature (Negrea et al., 2022) . Immune complexes were detected using chemiluminescence and protein expression levels were quantified by densitometry using Image Lab Software 4.1 (Bio-Rad) (Taylor et al., 2013) . Each protein expression level in the spheroids receiving a single DOX treatment was represented as fold change (FC) relative to the corresponding protein expression level in lysates from the control spheroids, and each was assessed in duplicate (Sezer et al., 2019).

Matrix Metalloprotease Activity Detection by Gelatin Zymography

The culture medium from DOX-treated and control spheroids group was collected and centrifuged at 350 x g for 5 min, to remove cell debris (Mrówczyńska et al., 2022). Protein concentration in the supernatant was determined by Bradford assay, followed by treatment with non-reducing buffer (4% SDS, 20% glycerol, 0.01% bromophenol blue, 125 mM Tris-HCl, H2O) (Bradford, 1976). Thereafter, 50 µg proteins/group were separated *via* SDS-PAGE, under non-reducing conditions, using a polyacrylamide 7.5% separation gel containing 0.1% gelatin (Licarete et al., 2020; Toth & Fridman, 2001). Following electrophoresis, the gels were washed to remove SDS and incubated overnight at 37°C in incubation buffer, to allow the gelatinase reaction to occur. The following day, the gels were stained with Coomassie blue solution for one hour, then destained with a solution containing 40% methanol and 10% acetic acid, until clear bands, corresponding to gelatinolytic activity of MMPs became visible. Enzyme activity areas were quantified through densitometry analysis using Image Lab Software 4.1 (Bio-Rad) (Taylor et al., 2013). The experiment was conducted in duplicate.

Apoptosis array

To detect the levels of expression of various apoptotic proteins in spheroids receiving a single DOX treatment and control spheroids, RayBio® Mouse Apoptosis Antibody C1 array (RayBiotech, Inc., Norcross, GA, USA) was performed according to the manufacturer's protocol (Leo et al., 2019). 38 proteins were screened by this array, among them 24 pro-apoptotic and 14 anti-apoptotic. The membranes were incubated with 250 µg of proteins of spheroids lysates, at 4 °C overnight, and subsequently for 2 hrs with primary biotinylated antibody cocktail specific for the apoptotic proteins, diluted 1:1000, followed by 2 hrs HRP-streptavidin incubation at room temperature. Formed immunocomplexes were detected by chemiluminescence, followed by image acquisition and densitometry analysis using Image Lab Software 4.1 (Bio-Rad). Protein expression levels in the DOX-treated group were expressed as fold changes (FC) relative to the corresponding levels in lysates from the control group, with each measurement assessed in duplicate (Sezer et al., 2019).

Statistical analysis

All data obtained from different experiments were reported as mean ± SD. GraphPad Prism version 7 for Windows (San Diego, CA, USA) was used to conduct all statistical analyses. The IC50 value for DOX was determined by non-linear regression of the sigmoidal dose-response curves using GraphPad Prism. IC30 value was calculated in Excel using the following formula: ICx=[(x/100-x)^1/Hillslope]*IC50, where x is % inhibition, Hillslope is the coefficient for the linear part of the curve, and IC50 is the concentration of the inhibitor causing 50% inhibition (Srinivasan & Lloyd, 2024) . Unpaired Student's t-test was used to statistically compare the effects of DOX administrations on the expression level of specific mRNAs and proteins. A *p*-value lower than 0.05 was defined as significant.

Results

Characterization of B16.F10 melanoma spheroids treated with doxorubicin at sub-inhibitory concentration

Based on the APH viability assay, the IC50 value of DOX was determined **(Figure 2A**), along with its corresponding sub-inhibitory IC30 value (0.282 µM), which was used for futher experiments involving DOX exposure. Melanoma spheroids were subjected to two consecutive exposures to DOX (0.282 µM), each followed by a 48-hour recovery phase, as illustrated in **Figure 2B** (Fey et al., 2020b; Kuczynski et al., 2013) . Representative images captured over the 10-day experimental period showed morphological changes in spheroids throughout the treatment (**Figure 2C**). To characterize spheroids growth throughout the experiment, the volume of spheroids from daily independent measurements was determined and used for the calculation of growth rate for each treated ($k_{DOX1,2}$) and untreated spheroids ($k_{CTR1,2}$) (**Figure 2E**). The normalized growth rate ($k_{DOX1,2}/k_{CTR1,2}$) was used to monitor the effects of drug treatment and evolution of drug resistance in spheroids (**Shahi Thakuri et al.,**

2019). Our results presented in **Figure 2E** showed that first exposure to DOX at a concentration of 0.282 uM significantly reduced the spheroid growth rate compared to that of the control spheroids ($p<0.001$) likely due to decreased viability of B16.F10 melanoma cells (**Figure 2D**). Moreover, the cell viability and the grow rate of the spheroids treated twice with DOX was significantly lower compared to corresponding control spheroids ($p<0.01$; **Figure 2D-F**) indicating cells in the 3D model retained their sensitivity towards DOX. Moreover, the resistance growth marker (K_{DOX2}/K_{CTR2}) of 0.098, which is below 1, confirmed that the cells remained sensitive to DOX, after the two exposures to DOX treatment (**Figure 2E**).

Transcriptional changes associated with the response of B16.F10 melanoma spheroids to DOX

To investigate gene and pathway alterations associated with drug resistance in B16.F10 melanoma spheroids following a single DOX exposure, RNA-seq analysis was conducted. DEGs were identified using a FR of ± 2, FDR < 20%, and $p < 0.05$ as cut-off criterias. A total of 1040 DEGs were detected, with 520 genes upregulated and 520 downregulated compared to control (**Supplementary Table 2,** Mendeley Data (Negrea et al., 2025)). DEGs were visualized using a hierarchical heatmap (**Figure 3A**), Volcano plot (**Figure 3B**), and Bar plot (**Figure 3C**). GO enrichment analysis (**Figure 3D**) linked DEGs to key biological processes, including cell cycle (GO:0007049), DNA damage response (GO:0006974), DNA repair (GO:0006281), and angiogenesis (GO:0001525), all of which were downregulated (**Supplementary Table 3.1**, Mendeley Data (Negrea et al., 2025)). KEGG pathway analysis (**Figure 3E**) revealed nine significantly altered pathways, with seven downregulated (e.g., cell cycle (mmu04110), DNA replication (mmu03030), and TNF-signaling (mmu04668)) and two upregulated (p53 signaling (mmu04115) and NOD-like receptor signaling (mmu04621)) (**Supplementary Table 3.2**, Mendeley Data (Negrea et al., 2025)). Gene Set Enrichment Analysis (GSEA) identified six enriched gene sets, with five negatively enriched (HALLMARK-G2M-CHECKPOINT, HALLMARK-E2F_TARGETS, HALLMARK-MITOTIC_SPINDLE, TNFA_SIGNALING_VIA_NFKB, and MTORC1_SIGNALING) and one positively enriched (INTERFERON_ALPHA_RESPONSE) (**Figure 4, Supplementary Figure 1, Supplementary Table 4**, Mendeley Data (Negrea et al., 2025)). Heatmaps (**Figures 4B-G**) illustrate mRNA expression patterns, with downregulation in cell cycle-related pathways and TNF-signaling pathways and upregulation in interferon alpha response genes, highlighting transcriptional changes upon first DOX exposure compared to control. Thereafter, we constructed a hierarchical representation of DEGs involved in the processes of interest (cell cycle, DNA damage and repair, apoptosis, angiogenesis, migration). As illustrated in the **Figure 5A**, the data revealed that all investigated processes were affected following a first exposure to DOX (0.282 µM). A subset of DEGs related to key biological processes of interest - cell cycle regulation (Cyclin-Dependent Kinase 1 (*CDK1*), NIMA-Related Expressed Kinase 2 (*Nek2*), Mitotic Arrest Deficient-Like 1 (*Mad2l1*), TopBP1 Interacting Checkpoint and Replication Regulator (*Ticrr*), and BUB1 Mitotic Checkpoint Kinase (*Bub1*)), DNA damage/repair (RecQ-mediated genome instability protein 2 (*Rmi)*, Histone 1X), apoptosis (stratifin (*Sfn*), cyclin G1), angiogenesis/migration (aquaporin 1 (*Aqp1)*, vascular endothelial growth factor (*VEGF*)) and migration (atypical chemokine receptor 3 (*Ackr3*), matrix metallopeptidase 9 (*MMP-9*)) was analyzed by RT-qPCR to validate transcriptomics findings. The results confirmed that RNA-seq data expression patterns aligned with RT-qPCR expression, showing consistent upregulation or downregulation of the same genes (**Supplementary Figure 2; Supplementary Table 5,** Mendeley Data (Negrea et al., 2025)). From all investigated processes following the first DOX exposure, cell cycle regulation and DNA damage response/repair had the most significant alterations in both in terms of the number of DEGs and the magnitude of expression changes (**Figure 5.1A; Supplementary Table 5**, Mendeley Data (Negrea et al., 2025)).

DOX treatment suppressed 172 cell cycle-related genes (with only 17 upregulated) (**Figure 5.1B**). Notably, critical regulators such as *CDK1, Nek2, Mad2l1, Ticrr, Bub1* were downregulated, while Cyclin-Dependent Kinase Inhibitor 1A (*CDKN1A/p2*1) and Proline/Serine-Rich Coiled-Coil 1 (*Psrc1*) were upregulated, suggesting impaired cell cycle progression (**Figures 5.1C,D**; **Supplementary Table 5,** Mendeley Data (Negrea et al., 2025)). GSEA analysis further supported that a single DOX exposure effectively inhibits normal cell cycle progression, contributing to its cytotoxic effects (**Figure 4**). After a second DOX exposure, RT-qPCR analysis of selected genes-*CDK1, NEK2, Cdc20, Bub1, Mad2l1, Ticrr, and Cyclin G1*-revealed that while *CDC20* and *Ticrr* remained downregulated, *CDK1, Nek2, Bub1*, and *Mad2l1* showed a slight increase in expression, approaching control levels (S**upplementary Figure 2A-**

F, Mendeley Data (Negrea et al., 2025)). Additionally, *Cyclin G1*, a cell cycle inhibitor with a pro-apoptotic role, was significantly lower after the second exposure compared to the first (**Supplementary Figure 2G,** Mendeley Data (Negrea et al., 2025)). These findings suggest that repeated DOX exposure may trigger adaptive transcriptional changes that support cell cycle progression.

Following the first DOX exposure, DNA damage response and repair mechanisms were severely disrupted (**Figure 5.1E-G; Supplementary Table 5,** Mendeley Data (Negrea et al., 2025)). The topoisomerase II alpha (*TOP2A*) gene was strongly downregulated along with 150 DEGs related to DNA damage (**Figure 5.1E**). Of these, DNA damage response had 64 transcripts including cell division cycle 45 (*Cdc45*), forkhead box M1 (*Foxm1*), Fanconi anemia complementation group D2 (*Fancd2*), exonuclease 1 (*Exo1*), BRCA1 interacting protein C-terminal helicase 1 (*Brip1*), BRCA1 associated RING domain 1 (*Bard1*), and RAD51 recombinase (*Rad51*) downregulated, suggesting disrupted replication, increasing DNA damage and impairing division, while 17 transcripts (e.g., three prime repair exonuclease 1(*Trex1*), etoposide-induced 2.4 (*EI24*), and sestrin 2 (*Sesn*)) were upregulated, indicating a possible compensatory response (**Figures 5.1 F,G**; **Supplementary Table 5**, Mendeley Data (Negrea et al., 2025)). Our results suggest impaired DNA repair and genomic instability, with 51 DEGs-including DNA polymerase theta (*Polq*), poly(ADP-ribose)-binding protein (*Parpbp*), and Fanconi anemia complementation group I (*Fanci*) downregulated, while only 4 DEGs upregulated (**Figure 5.1 F,G; Supplementary Table 5,** Mendeley Data (Negrea et al., 2025)). Notably, after a second DOX exposure, *Rmi2* mRNA expression doubled ($p < 0.05$) compared to control (CTR2), whereas it was downregulated ($p < 0.05$) relative to the first control (CTR1), as confirmed by RT-qPCR (**Supplementary Figure 2H**, Mendeley Data (Negrea et al., 2025)).

Apoptosis-related pathways exhibited significant transcript expression changes, with 106 DEGs identified (**Figure 5.2 H**). Both extrinsic and intrinsic apoptotic signaling were suppressed, as shown by the downregulation of survivin (*Birc5*) and BCL2-related ovarian killer (*Bok*), while p53-induced death domain protein 1 (*Pidd1*) was upregulated (**Figure 5.1 I,J; Supplementary Table 5**, Mendeley Data), indicating reduced apoptosis initiation. TNFA_SIGNALING_VIA_NFKB (**Figure 4E**) is a well-known pathway involved in apoptosis regulation (Aggarwal, 2004; Amiri & Richmond, 2005) . Following a second DOX exposure, RT-qPCR analysis revealed that *Sfn* - a direct target of p53 involved in the intrinsic apoptotic signaling pathway in response to DNA damage, transcript expression returned to control level (CTR2) but was still significantly lower ($p < 0.05$) than after a single DOX exposure (**Supplementary Figure 2J,** Mendeley Data (Negrea et al., 2025)). Meanwhile, pro-apoptotic genes Bcl-2-associated X protein *(Bax)* and Bcl-2-interacting domain death agonist *(Bid)* were unchanged ($p>0.05$), and the anti-apoptotic B-cell lymphoma 2 *(Bcl-2)* decreased slightly ($p < 0.05$) after the second exposure (**Supplementary Figure 2 K-M**, Mendeley Data (Negrea et al., 2025)).

Angiogenesis was notably affected, with 46 DEGs identified (31 downregulated, 15 upregulated) (**Figures 5.2 K,L**). DOX upregulated Bone marrow stromal cell antigen 2 (*Bst2*) and EGF and pentraxin domain containing 1 (*Svep1*) - both linked to pro-angiogenic signaling, while downregulating ephrin type-A receptor 2 (*Epha2*) and cellular communication network factor 6 (*Ccn6*), which are involved in vascular development and stabilization (**Figure 5.2 L,M**). The mTORC1 and TNF-α/NF-kB signaling pathways, enriched in GSEA analysis (**Figure 4 D,E**), play key roles in regulating angiogenesis and inflammation (Amiri & Richmond, 2005; S. Huang et al., 2001; H. Li et al., 2022; Noort et al., 2014; Thiem et al., 2013). Following a second DOX exposure, RT-qPCR analysis revealed significant upregulation of *VEGF* and *Aqp1* ($p < 0.05$) in spheroids treated twice with DOX (DOX2), compared to both the control (CTR2) and the single DOX- treatment group (DOX1) spheroids (**Supplementary Figure 2 O,P**, Mendeley Data (Negrea et al., 2025)).

Migration and invasion-related transcripts were equally up and downregulated after the first exposure to DOX, comprising a total of 96 DEGs (**Figure 5.2 N,O; Supplementary Table 5**, Mendeley Data). Several protocadherins and adhesion-related genes were upregulated, while key mediators of cell-cell interactions *Nectin4*, cadherin-6 (*Cdh6*), and integrin alpha-3 (*Itga3*) were downregulated (**Figure 5.2 O,P**). Notably, matrix metalloproteinase-9 (*MMP-9*), a critical EMT driver (Tune et al., 2022), was 2-fold suppressed ($p < 0.001$), whereas matrix metalloproteinase-

15 (*MMP-15*) was upregulated 11-fold ($p < 0.001$), suggesting a shift toward MMP-15 mediated ECM remodeling. Additionally, DOX increased *Notch1* expression and upregulated transcripts associated with tumor aggressiveness-namely, tumor necrosis factor receptor superfamily member 19 (*Tnfrsf19*), plexin domain-containing protein 2 (*Plxdc2*), interleukin-16 (*IL-16*), and angiopoietin-like 2 (*Angptl2*) with the TNF-α-induced NF-kB pathway also implicated in enhanced invasion (**Figures 4E and 5.2 N-P**) (Y. Wu & Zhou, 2010; Xia et al., 2014). Finally, RT-qPCR after the second DOX exposure revealed increased *MMP-2* expression, unchanged *MMP-9* expression, and consistent upregulation of *Ackr3* after both DOX exposures compared to control (**Supplementary Figure 2 Q-S,** Mendeley Data (Negrea et al., 2025)). Therefore, following a first exposure to DOX, most of the transcripts evaluated involved in key tumor progression processes were downregulated compared to control. However, most of these changes were not maintained after the second DOX, as the evaluated genes showed mRNA expression levels more similar to those in the first control spheroids, prior to treatment, suggesting that the cells initiated transcriptional compensatory mechanisms in response to repeated DOX exposure.

Investigation of the effects of repeated exposure to DOX on main tumor progression processes in 3D melanoma model at protein level

To investigate whether the effects of DOX noticed on mRNA transcripts were maintained at the protein level in B16.F10 melanoma spheroids, we analyzed the expression of key proteins involved in apoptosis, angiogenesis, and migration and a main related transcription factor by western blot, protein array, and gelatinase assay (**Figure 6)**.

Based on GSEA analysis, the TNFA_SIGNALING_VIA_NFKB pathway (**Figure 4E**) was significantly negatively enriched in spheroids after first exposure to DOX compared to the control. Since NF-kB is a key transcription factor involved in proliferation, survival, and resistance mechanisms, we assessed the expression levels of phosphorylated NF-kB (pNF-kB) in both DOX-exposed and control spheroids (Godwin et al., 2013; Meylan et al., 2009). While NF-kB mRNA expression remained unchanged after the first DOX exposure, pNF-kB protein expression was significantly reduced by 50% in spheroids exposed once to DOX compared to control (**Figure 6A**). We then re-evaluated its expression after the second exposure to DOX (**Figure 6A)**. Notably, pNF-kB levels were comparable between spheroids exposed twice to

DOX and control spheroids (CTR2) ($p>0.05$) but increased by 40% compared to its level after the initial exposure to DOX ($p<0.05$) (**Figure 6A**). These results suggest that the second exposure to DOX may have triggered adaptive cellular responses in melanoma model involving NF-kB activation and potentially NF-kB-regulated pathways.

Since RNA-seq analysis revealed significant modulation of transcripts encoding apoptosis-related proteins, with both upregulated and downregulated transcripts (**Supplementary Table 5**, Mendeley Data (Negrea et al., 2025)), we further evaluated the expression levels of key apoptotic proteins in B16.F10 melanoma spheroids after the first DOX exposure by assessing 38 apoptotic proteins using a C1 apoptosis protein array (**Figure 6B**). Our findings show that both a pro-apoptotic and an anti-apoptotic protein were significantly regulated in response to first exposure to DOX treatment (**Figure 6B; Table 1)**. Among the 38 proteins, 9 proteins were not expressed in sufficient amount in either control or DOX-exposed spheroids, namely Bcl-2-like protein 2 (BCL-W), Insulin-like growth factor-binding protein 6 (IGFBP-6), Insulin-like growth factor 2 (IGF-2), p21 (Cip1/Waf1), CD40 Ligand (CD40L), Tumor Necrosis Factor Receptor I (TNF RI, TNFRSF1A), Tumor Necrosis Factor Alpha (TNFα), and TNF-Related Apoptosis-Inducing Ligand Receptor 2 (TRAIL R2, TNFRSF10B), second mitochondria-derived activator of caspase (SMAC) (pro-apoptotic proteins). The mRNA expression of these proteins remained unaffected after initial DOX exposure. Among the 19 pro-apoptotic proteins detected in the array, only Bax protein expression significantly increased by 2-fold ($p < 0.05$) in spheroids after the first DOX exposure compared to the control, while the other proteins had similar expression level to those noticed in the corresponding control group (**Figure 6B; Table 1**). Interestingly, similar results were identified for the 10 anti-apoptotic proteins detected, as cIAP-2 protein was upregulated by 2-fold ($p < 0.05$), while for survivin, IGF-1, Bcl-2, Heat shock protein 70 (HSP70), IGFBP-1, IGFBP-2 and X-linked Inhibitor of Apoptosis Protein (XIAP) the expression levels after the first DOX exposure was not statistically different compared to the control group protein expression levels (**Figure 6B; Table 1**). Except for the suppressed transcription of pro-apoptotic *survivin* gene by 3-fold ($p<0.01$), all the other protein encoding transcripts had unchanged expression after DOX exposure (**Supplementary Table 5**; **Supplementary Figure 2 J-M,** Mendeley data (Negrea et al., 2025)). However, because the protein expression of both an activator (Bax) and an inhibitor (cIAP-2) of apoptosis had been favored by DOX-treatment, the cancer cells might have attempted to balance cell death and survival in response to the administration of the sub-inhibitory DOX concentration, and apoptosis was probably not initiated. Based on our RNA-seq data that indicated transcripts encoding for proteins involved in angiogenesis were significantly modulated in both upregulating and downregulating manner (**Supplementary Table 5,** Mendeley Data (Negrea et al., 2025)), we further chose to evaluate the protein expression levels of the most common 24 angiogenic and inflammatory proteins through C1 protein array in spheroids after the first exposure to DOX, compared to control. Thus, the production of 10 out of 24 proteins was significantly changed in spheroids exposed to DOX, compared to control spheroids. As represented in **Figure 6C and Table 2,** DOX administration increased the levels of protein expression of the following pro-angiogenic and pro-inflammatory proteins by 2-fold: eotaxin-1 ($p<0.001$), Interleukin-1β (IL-1β, $p<0.05$), Monocyte Chemoattractant Protein-1 (MCP-1, $p<0.01$), Interleukin-1α (IL-1α, $p<0.01$), Interleukin-6 (IL-6, $p<0.05$), Interleukin-9 (IL-9, $p<0.05$), Interleukin-13 (IL-13, $p<0.01$), Macrophage Colony-Stimulating Factor (M-CSF, $p<0.01$), and VEGF ($p<0.05$) compared with their production in the control group, except for Fas Ligand (FasL), Granulocyte Colony-Stimulating Factor (G-CSF), Granulocyte-Macrophage Colony-Stimulating Factor (GM-CSF), Insulin-Like Growth Factor 2 (IGF-2), Interleukin-12 (IL-12), and Thrombopoietin (TPO), which had similar expression levels compared to the expression in the control spheroids. Among the anti-angiogenic proteins evaluated in the protein array, only Tissue Inhibitor of Metalloproteinases-1 (TIMP-1) expression level significantly increased by 1.7-fold ($p<0.05$) in spheroids exposed to DOX compared to their expression in the control spheroids, while Platelet Factor 4 (PF4), Monokine Induced by Gamma Interferon (MIG) and TIMP-2 had similar expression levels as found in the control spheroids (**Figure 6C and Table 2**). Except for *VEGF* which showed a -1.84-fold decrease in mRNA expression according to our RT-qPCR (below the 2-fold cutoff chosen for RNA-seq analysis), the other protein encoding genes investigated in this protein array were not affected at the mRNA level by the exposure to DOX. These findings suggest angiogenesis and inflammatory responses signaled by these significantly modified molecules were favored by the first exposure to sub-inhibitory concentration of DOX.

According to the RNA-seq data, we observed migration potential was affected by the first exposure to DOX, having both upregulated and downregulated-transcripts encoding for proteins in this process (**Supplementary Table 5**, Mendeley Data (Negrea et al., 2025)), we assessed the activity of MMP-2 and MMP-9 - enzymes linked with invasion/metastasis potential and cancer drug resistance, in the culture medium collected from the spheroids *via* gelatin zymography (**Figures 5.2 N-P and 6D**) (Henriet & Emonard, 2019; Qian et al., 2020) (Kunz et al., 2016; Spallarossa et al., 2006). Our data showed that the first DOX exposure had no significant effect on MMP-2 activity or mRNA expression compared to the control ($p>0.05$, **Supplementary Figure 2,** Mendeley data (Negrea et al., 2025) **and Figure 6E**). However, after the second exposure, MMP-2 activity remained unchanged compared to its control group (CTR2) ($p>0.05$), but it increased by 15% compared to spheroids receiving a single DOX exposure ($p<0.05$, **Figure 6E**). In both single and double DOX-exposed spheroids, MMP-9 activity was significantly elevated compared to controls ($p<0.05$), with no significant difference between exposures ($p>0.05$), while mRNA expression was lower than in controls (**Figure 6D; Supplementary Figure 2S; Supplementary Table 5,** Mendeley Data (Negrea et al., 2025)).

Overall, these findings suggest that the exposure of 3D melanoma spheroids to the sub-inhibitory concentration of DOX has cytotoxic effects but triggers complex cellular adaptations, including changes in key pathways involved in cell survival and migration, to promote an early acquired resistance to DOX.

Discussion

This study aimed to identify the mechanisms linked to the early settlement of DOX resistance, as well as the associated processes, in B16.F10 murine melanoma cells, following repeated exposure to a sub-inhibitory concentration (IC30) of the cytotoxic drug. To accomplish this goal, B16.F10 melanoma cells were grown as spheroids, since 3D culturing of cells is known to modulate cellular responses to cytotoxic agents and better mimic chemoresistance observed in vivo (Filipiak-Duliban et al., 2022; Kunz-Schughart et al., 1998). By utilizing this model, early resistance markers were identified, offering valuable insights for the early detection of DOX resistance and aiding the development of more effective therapeutic strategies.

RNA-seq provided evidence that, an initial exposure of B16.F10 melanoma spheroids to DOX, led to downregulation of *TOP2A* mRNA expression compared to its expression in the control spheroids (**Supplementary Table 4,** Mendeley Data (Negrea et al., 2025)), without significant alteration of standard ABC transporters transcripts involved in DOX efflux (Filipiak-Duliban et al., 2022; Liu, 1989; Nitiss, 2009) . *TOP2A* inhibition in DOX-treated B16.F10 melanoma spheroids triggered an adaptive response, altering cell cycle dynamics. This was evidenced by the suppression of pathways related to cell cycle progression (downregulation of *CDK1, Nek2, Mad2l1, Bub1* or *Ticrr* transcripts), proliferation, and survival, as confirmed by RNA-seq data and GSEA analysis **(Figures 4A-D and 5.1; Supplementary Figure 2 A-F; Supplementary Table 5,** Mendeley Data (Negrea et al., 2025) **)**. Additionally, a significant reduction in DNA repair capacity, particularly in homologous recombination (HR) and topoisomerase-induced damage genes, was observed **(Figure 5.1 E-G; Supplementary Figure 2 H,I; Supplementary Table 5,** Mendeley data (Negrea et al., 2025)**)** (Albertson et al., 2009; Chae et al., 2019; Keijzers et al., 2018; Sertic et al., 2011; Singh et al., 2008; Thorn et al., 2011; J. Y. J. Wang, 2019; Xie et al., 2020) . These changes suggest that DOX exposure arrested B16.F10 melanoma cells at key cell cycle checkpoints (G1/S, G2/M, and M) (Karthikeyan et al., 2024).

Since homologous recombination occurs mainly in S and G2 phases (Branzei & Foiani, 2008), our results might imply that melanoma cells accumulated in the G2/M checkpoint, being unable to proceed to mitosis (**Supplementary Table 5, Supplementary Figure 2,** Mendeley data (Negrea et al., 2025)) (Vera et al., 2015) . This hypothesis is further supported by downregulation of *FOXM1, Fanci, Pola1 POLα, Polq POLθ,* and *Pole* transcripts in spheroids after first exposure to DOX (**Supplementary Table 5,** Mendeley data (Negrea et al., 2025)), which could result in genomic instability due to inefficient DNA repair (Liddiard et al., 2022; Osrodek & Wozniak, 2021) , and could explain the reduced cell viability and spheroids growth (**Figure 2A**). However, after an initial exposure to the cytotoxic drug, cancer cells could re-enter the cell cycle, leading to tumor relapse (Matt & Hofmann, 2016; Singvogel & Schittek, 2024; J. Y. J. Wang, 2019). Following the second exposure to DOX of the melanoma spheroids, RT-PCR data confirmed that the expression level of some of the resistance transcripts associated with cell cycle dynamics (*CDK1, Nek2, Mad2l1, Histone 1* and *cyclin G1*) reverted to control levels (**Supplementary Figure 2 A-G**, Mendeley data (Negrea et al., 2025)) (AbuHammad & Zihlif, 2013; Tormo et al., 2019) , while the expression of *Bub1* and *Rmi2* genes were upregulated (**Supplementary Figure 2 D,H,** Mendeley data (Negrea et al., 2025)) (Y. Li et al., 2022; Xiao et al., 2020; Zhan et al., 2020) . Collectively, these data indicate that melanoma cells might have bypassed the cell-cycle checkpoints after first DOX exposure (Christowitz et al., 2019; Visconti et al., 2016) , while their ability to reform the spheroids and maintaining drug sensitivity after second DOX exposure reflects acquiring of a transient chemoresistant phenotype (Rambow et al., 2019) (**Supplementary Figure 2,** Mendeley data (Negrea et al., 2025) **and Figure 1 and 2)**. Under conditions of pronounced DNA damage and impaired repair capacity, cells attempting mitosis are susceptible to genomic instability, and prone to cell death (Castedo et al., 2004; Ryl et al., 2017).

Our mRNA analysis results revealed that in response to a first DOX exposure, both intrinsic and extrinsic apoptotic signaling pathways as well as pro-apoptotic factors (e.g., *Bok*) showed predominant downregulation in B16.F10 melanoma spheroids, with *p21, Sfn, Pidd1* transcripts being upregulated (**Figure 5.2 H-J**; **Supplementary Table 5,** Mendeley data (Negrea et al., 2025)). Inhibition of TNF-α signaling would typically reduce apoptosis mediated by this pathway (**Figure 4E**) (Micheau & Tschopp, 2003) . At protein level, the expression of death-related proteins such as Fas, FASL, Cytochrome C, and growth arrest mediators IGFBP and p27, remained similar to that noticed in the control spheroids (**Figure 6B**, **Table 1**). In contrast, the protein expression of anti-apoptotic cIAP2 that inhibits caspases (Cas-3, Cas-6) activity, was increased, pointing to initiation of early apoptotic events in spheroids after first exposure to DOX without progressing to downstream execution phase (**Figure 6B**, **Table 1)** (Esposito et al., 2007; Kavanagh et al., 2014). Moreover, these modifications were not associated with upregulation of the *TP53* gene, despite the cell line maintaining functional wild-type p53 (Melnikova et al., 2004). Nonetheless, the significant increase in mRNA expression of *p21,* of *cyclin G1,* and other p53-responsive transcripts, simultaneously with the positive enrichment of the p53 signaling pathway identified by our KEGG functional analysis, but accompanied by increased anti-apoptotic cIAP2 protein expression reinforced the observation that the extent of pro-apoptotic events induced by DOX was not sufficient to fully commit B16.F10 melanoma cells to apoptosis (**Figure 3E**; **Supplementary Table 3.2,** Mendeley Data (Negrea et al., 2025)). These findings support a scenario where melanoma cells were maintained in a prolonged state of cell cycle arrest (Beaumont et al., 2016) (**Supplementary Table 5,** Mendeley data (Negrea et al., 2025)), which may have provided time for DNA repair before mitosis or enabled some of the melanoma cells exposed to DOX to bypass cell cycle checkpoints, likely relying on error-prone DNA repair pathways (Kaufmann et al., 2008) , as indicated by downregulation of *Rad51* mRNA, a key regulator of homologous recombination. (**Supplementary Table 5**, Mendeley Data (Negrea et al., 2025)) (Gordon et al., 2018; Jensen et al., 1998; Kimura et al., 2001; Kimura & Nojima, 2002; Okamoto et al., 1996; Okamoto & Beach1, 1994).

The second exposure to DOX might have induced apoptosis in B16.F10 melanoma cells via *Bcl-2* downregulation ($p<0.05$), though reduced *cyclin G1* mRNA expression noticed in spheroids treated twice with DOX, compared to those receiving a single DOX treatment ($p<0.05$) may have counteracted this effect (**Supplementary Figure 2 G,M; Supplementary Table 5**, Mendeley data (Negrea et al., 2025)).

Collectively, these results describe an early settlement of DOX-induced resistance in B16.F10 melanoma spheroids, through cell-cycle adaptation and apoptotic escape, allowing the melanoma cells to survive under severe DNA damage and defective DNA repair systems, by activating alternative survival pathways (S. Wu & Singh, 2011). Thus, the inhibition of the key pro-survival mTOR, NF-kB, and TNFα via NF-kB signaling pathways in B16.F10 melanoma spheroids receiving a single DOX treatment, were counteracted by increasing *Notch1* mRNA expression ($p<0.001$) (**Figure 4A,E,F; Supplementary Tables 4, 5** Mendeley Data (Negrea et al., 2025)), shifting cells phenotype from a highly proliferative (mTOR/NF-kB-driven) to a quiescent-like/

invasive phenotype (Notch1-driven) (Z. Wang et al., 2010) . Notch 1-driven adaptation was supported by complex upregulation of mRNA genes involved in cell proliferation/survival (*Tnfrsf19* receptor), angiogenesis (*Aqp1* and *Angpt2*) (Deng et al., 2023; Guo et al., 2024; Paulino et al., 2010), intercellular junction formation (*Pcdh* beta 5, 7, 9, 10, 11, 12, 14) (Endo et al., 2012; Guan et al., 2021; Kadomatsu et al., 2014; Lang et al., 2023; Masuda et al., 2015; B. Wu et al., 2022) or ECM remodeling (*CDH1*, *Itgal*, *Cercam*, *Ecm1*, *Chl1,* as well as *MMP-15* and *Jam2*) (**Supplementary Table 5,** Mendeley Data) (Berx & van Roy, 2009; H. F. Chen et al., 2017; A.-M. Li et al., 2013; Meguenani et al., 2015; Mukai et al., 2017; Zheng et al., 2023; Zhu et al., 2014). Despite the downregulation of *VEGF* and *MMP-9* transcripts in B16.F10 melanoma spheroids receiving a single DOX exposure (**Supplementary Figure 2 N,R**, Mendeley data (Negrea et al., 2025)), overexpression of corresponding proteins expression/activity (**Figure 6C,D**) as well as of IL-1β, IL-1α, Eotaxin-1, IL-6, IL-9, M-CSF, MCP-1 and TIMP-1 indicated that cancer cells might favor the maintenance of adequate levels of essential proteins to enable growth and dissemination, most probably by post-transcriptional regulatory mechanisms (**Supplementary Table 4:** Mendeley Data (Negrea et al., 2025) ; **Table 2)** (Mantovani et al., 2018) . Notably, the second exposure of melanoma spheroids to DOX, further activated angiogenic signaling mediated by upregulation of *VEGF*, *Aqp1* or *Ackr3* transcripts, and of MMP-2/9, at mRNA and protein level, highlighting a key mechanisms of adaptive resistance, that enabled cancer cells to withstand DOX-induced damage and acquire a more aggressive phenotype (Henriet & Emonard, 2019; Kunz et al., 2016; Qian et al., 2020; Spallarossa et al., 2006) (**Supplementary Table 5,** Mendeley Data (Negrea et al., 2025); **Figures 1N-R and 6D**) (Antonello et al., 2023; Chern & Tai, 2020; Duval et al., 2022). These findings offer a valuable opportunity to develop targeted therapeutics, by associating DOX with agents that inhibit cell-cycle progression, angiogenesis and the aggressiveness of melanoma cells, in order to overcome resistance (Licarete et al., 2019, 2020; Negrea et al., 2022).

Conclusion

In summary, we describe here a mechanism of early adaptation of B16.F10 melanoma spheroids to DOX, associated with the arrest of cells at G1 to S, G2 to M, and M cell-cycle checkpoints. Despite experiencing major DNA damage and having impaired DNA repair mechanisms, these cells evaded apoptosis and bypassed the cell-cycle checkpoints by upregulating transcripts encoding for proteins that promote angiogenesis, cell adhesion and ECM remodeling, favoring dissemination, as showed by upregulation of transcripts such as *Tnfrsf19, Aqp1, Angpt2, MMP-15, Jam2* and enhanced expression of VEGF, eotaxin-1, M-CSF proteins and of MMP-9 activity. Following a second DOX exposure, these cells engaged in compensatory/alternative survival pathways, driven by NF-kB, that led to positive regulation of angiogenesis and migration-related pathways, through increased mRNA expression of *VEGF, MMP-2, Apq1, Ackr3* transcripts and of MMP2/9 enzyme activity indicating the acquisition of a transient drug resistance and more aggressive phenotype. Future studies should explore the long-term effects of DOX exposure on melanoma cells in 3D culture in the presence of other stromal cells, to better understand how the complex cellular cross-talk in TME or its heterogeneity contributes to chemoresistance, in order to identify potential therapeutic targets.

This article contains supplemental data available at Mendeley Data: **Negrea et al, 2025;** doi: 10.17632/248c3t93fz.1

Declaration of generative AI in scientific writing

The authors acknowledge the use of generative AI (ChatGPT 3.5) in enhancing the readability and language of the manuscript. After using the tool, the authors thoroughly reviewed and edited the content, taking full responsibility for the final manuscript.

Tables and Figures

Table 1. Protein expression of angiogenic and inflammatory proteins in spheroids after the first exposure to DOX compared to control spheroids

Table 2. Protein expression of apoptotic proteins in spheroids after the first exposure to DOX compared to control spheroids

Figure 1. Experimental timeline and morphological assessment of growth and viability in B16.F10 melanoma spheroids exposed to DOX. A. Cell viability (%) of B16.F10 melanoma spheroids after multiple DOX treatments at

different concentrations assessed *via* APH assay. **B.** Schematic overview of the experimental protocol, consisting of two exposures to DOX with a single recovery phase in between, along with representative images showing the growth and morphology of the spheroids throughout the experiment (50× magnification, scale bar = 100 µm).

Figure 2. Characterization of growth and cell viability of B16.F10 melanoma spheroids exposed to DOX. A. Spheroids viability (%) after the first and second exposure to DOX treatment, compared to control (untreated) spheroids. **B.** Spheroids average growth rates during the two exposures to DOX treatment ($K_{DOX1,2}$) compared to control ($K_{CTR1,2}$) represented as mean ± SD and the growth rate resistance marker - K_{DOX}/K_{CTR} ratio. **F.** Graphical representations of growth rates of DOX-treated spheroids, of control spheroids, and K_{DOX}/K_{CTR} normalized growth rate. Results are presented as mean ± SD of three independent experiments (n=9). **: $p < 0.01$; ***: $p < 0.001$, ****: $p < 0.0001$, *ns*: not significant.

Figure 3. General overview of RNA-seq data analysis in spheroids after first exposure to DOX and control spheroids. A. Supervised hierarchical clustering analysis of differentially expressed genes (DEGs) in control (untreated) spheroids versus spheroids first exposed to DOX. The heatmap clusters 1040 DEGs based on normalized FPKM values. Each column represents a biological replicate/group (CTR1_1, CTR1_2 for control spheroids and DOX1_1, DOX1_2 for treated spheroids), with each row representing a specific transcript. Gene expression levels are displayed according to a color scale: red indicates an increase in transcript abundance (positive Z-scores; $0 <$ Z-score ≤ 1.5), blue represents a decrease (negative Z-scores; $-1.5 \leq$ Z-score < 0), and white shows median expression (Z-score close to zero). Genes with FR ± 2, $p < 0.05$, and FDR 20% were considered differentially expressed. The X-axis represents log2 fold change (up- or downregulation), and the Y-axis represents -log10(p-value) (statistical significance). **B.** Volcano plot showing DEGs in spheroids after first exposure to DOX compared to control (untreated) spheroids. Significant upregulated genes are shown in red, downregulated genes in blue, and non-significant genes in gray. **C.** Bar plot showing the number of upregulated and downregulated DEGs in spheroids after first exposure to DOX compared to control (untreated) spheroids. **D.** Bar plots highlighting the most enriched Gene Ontology (GO) terms for activated (left) and suppressed (right) processes in spheroids after first exposure to DOX compared to control (untreated) spheroids. GO terms are categorized into three colored groups: green for Biological Process (BP), red for Cellular Component (CC), and blue for Molecular Function (MF). The X-axis shows the number of genes per GO term, indicating enrichment levels. **E.** Dot plot of enriched KEGG pathways, showing suppressed (left) and activated (right) pathways in first DOX-treated spheroids compared to control (untreated) spheroids. R was used for the generation of all representations. **Abbreviations: DEGs**: differentially expressed genes; **FPKM**: Fragments Per Kilobase of transcript per Million mapped reads.

Figure 4. GSEA Hallmark analysis. Images are showing significant gene sets enrichment at FDR < 20% and a nominal *p*-value < 5% in control (untreated) spheroids compared to spheroids after first exposure to DOX **A**. Bar plot indicating the GSEA enriched pathways. A positive Normalized Enrichment Score (NES) value indicates enrichment in the control group, and a negative NES indicates enrichment in spheroids in spheroids after first

exposure to DOX. **B-G**. The corresponding heatmaps of the gene sets for control spheroids (left column) in comparison with spheroids in spheroids after first exposure to DOX (right column). Expression values are represented as colors and range from red (high expression), pink (moderate), light blue (low) to dark blue (lowest expression).

Figure 5.1 Analysis of RNA-seq data involved in selected processes in spheroids after first exposure to DOX and in control spheroids. A. Supervised hierarchical clustering analysis of DEGs considered of interest in spheroids after first exposure to DOX compared to the untreated spheroids. Heatmap Clustering of 339 DEGs was generated using normalized FPKM values. Each column represents a biological replicate/group (CTR1_1, CTR1_2 replicates of the gene expression in untreated spheroids and DOX1_1, DOX1_2 replicates of the gene expression in treated spheroids), and each row represents a specific transcript. **B-D. Diagrams representing data in Cell cycle**: **B.** Stacked bar chart of DEGs related to the process; **C**. Bar graph representing the distribution of genes; **D.** Heat Plot of significantly enriched pathways related to cell cycle in GO. **E-G. Diagrams representing data in DNA damage and repair response: E.** Stacked bar chart of all DEGs related to the process; **F**. Bar graph; **G**. Vulcano plot. Colors pattern: Blue (downregulated transcripts): Indicates the proportion of genes showing decreased expression in spheroids after first exposure to DOX compared to control, and Red (Upregulated): Indicates the proportion of genes showing increased expression in spheroids after first exposure to DOXcompared to control. R and Microsoft excel were used for these representations. **Abbreviations: DEGs**: differentially expressed genes; **FPKM**: Fragments Per Kilobase of transcript per Million mapped reads.

Figure 5.2 Analysis of RNA-seq data involved in selected processes in spheroids after first exposure to DOX and in control spheroids (5.1. continued). H-J. Apoptosis diagrams: **H**. Stacked bar chart; **I**: Bar plot representing the distribution of genes; **J.** Supervised hierarchical clustering analysis of DEGs involved in the process; Each column represents a biological replicate/group (CTR1_1, CTR1_2 replicates of the gene expression in untreated spheroids and DOX1_1, DOX1_2 replicates of the gene expression in treated spheroids), and each row represents a specific transcript. **K-M. Diagrams representing data in Angiogenesis**: **K.** Stacked bar chart; **L.** Supervised hierarchical clustering analysis of DEGs involved in the process; Each column represents a biological replicate/group (CTR1_1, CTR1_2 replicates of the gene expression in untreated spheroids and DOX1_1, DOX1_2 replicates of the gene expression in treated spheroids), and each row represents a specific transcript. **M.** Bar graph representing the distribution of genes. **N-P. Diagrams representing data in Migration: N.** Stacked bar chart; **O**. Bar plot representing distribution of genes**; P.** Vulcano plot. Colors pattern: Blue (downregulated transcripts): Indicates the proportion of genes showing decreased expression in spheroids after first exposure to DOX compared to control, and Red (Upregulated): Indicates the proportion of genes showing increased expression in first DOX-treated spheroids compared to control. R and Microsoft excel were used for these representations. **Abbreviation: DEGs:** differentially expressed genes.

Figure 6. Effects of repeated DOX exposure on protein expression/enzyme activity in B16.F10 melanoma spheroids. A. Western blot images and the corresponding graph showing the % of phosphorylated pNF-kB protein level in spheroids after first and after second exposure to DOX, compared to control (untreated) spheroids; β-actin was used as loading control. Data are represented as mean ± SD (n=3); ns: not significant; *$p < 0.05$, **$p < 0.01$. **B.** Production of pro/anti-apoptotic proteins in DOX-treated spheroids compared with the levels of the same proteins in control (untreated) spheroids. Results are presented as fold changes of reduction in protein levels ranging from 0 (white) to -1 (yellow), or as fold changes of increase in protein production ranging from 0 (white) to 2 (blue). **C.** Production of angiogenic/inflammatory proteins in spheroids after first exposure to DOX, compared with the levels of the same proteins in control (untreated) spheroids. Results are presented as fold changes of reduction in protein levels ranging from 0 (white) to -1 (yellow), or as fold changes of increase in protein production ranging from 0 (white) to 2 (purple). **D.** MMP-2 and MMP-9 activity profiles in spheroids after first and after second exposure to DOX, compared to activity of the same proteins in control spheroids, assessed by gelatin zymography. Percentage of clearance, represented as bar graphs, was obtained by normalizing the area of clearance of DOX-treated spheroids to its correspondent in control (untreated) spheroids.

Abbreviations: **BAD**: BCL-2-associated death promoter, **BAX**: BCL-2-associated X protein, **BCL-2**: B-cell lymphoma 2, **BCL-W**: BCL2-like 2, **bFGF**: basic fibroblast growth factor, **BID**: BH3-interacting domain death agonist, **BIM**: BCL-2-like 11, **Caspase-3**: cysteine-aspartic acid protease-3, **Caspase-8**: cysteine-aspartic acid protease-8, **CD40 (TNFRSF5)**: Cluster of Differentiation 40, **cIAP-2**: cellular inhibitor of apoptosis protein 2, **cytoC**: cytochrome C, **DR6 (TNFRSF21)**: Death Receptor 6, **Fas (apo-1)**: Fas cell surface death receptor, **FasL**: Fas ligand, **Fas Ligand (TNFSF6)**: Fas ligand, **G-CSF**: granulocyte-colony stimulating factor, **HSP27**: heat shock protein 27, **HSP60**: heat shock protein 60, **HSP70**: heat shock protein 70, **HTRA2**: high temperature requirement protein A2, **IFN**: interferon, **IGF**: insulin-like growth factor, **IGF-1**: insulin-like growth factor 1, **IGFBP-1**: insulin-like growth factor binding protein 1, **IGFBP-2**: insulin-like growth factor binding protein 2, **IGFBP-3**: insulin-like growth factor binding protein 3, **IGFBP-4**: insulin-like growth factor binding protein 4, **IGFBP-5**: insulin-like growth factor binding protein 5, **IL**: interleukin, **M-CSF**: macrophage-colony stimulating factor, **MMP**: matrix metalloproteases; p27: cyclin-dependent kinase inhibitor 1B, **NF-kB**: Nuclear factor kappa B, **p53**: tumor protein p53, **Survivin**: baculoviral inhibitor of apoptosis repeat-containing 5, **TIMP**: tissue inhibitor of metalloproteinase, **TNF**: tumor necrosis factor, and **VEGF**: vascular endothelial growth factor.

References

AbuHammad, S., & Zihlif, M. (2013). Gene expression alterations in doxorubicin resistant MCF7 breast cancer cell line. *Genomics*, *101*(4), 213–220. https://doi.org/10.1016/j.ygeno.2012.11.009

Aggarwal, B. B. (2004). Nuclear factor-κB. *Cancer Cell*, *6*(3), 203–208. https://doi.org/10.1016/j.ccr.2004.09.003

Ahmad, T., Lee, J., Shin, Y. M., Shin, H. J., Madhurakat Perikamana, S. K., Park, S. H., Kim, S. W., & Shin, H. (2017). Hybrid-spheroids incorporating ECM like engineered fragmented fibers potentiate stem cell function by improved cell/cell and cell/ECM interactions. *Acta Biomaterialia*, *64*, 161–175. https://doi.org/10.1016/j.actbio.2017.10.022

Albertson, T. M., Ogawa, M., Bugni, J. M., Hays, L. E., Chen, Y., Wang, Y., Treuting, P. M., Heddle, J. A., Goldsby, R. E., & Preston, B. D. (2009). DNA polymerase ε and δ proofreading suppress discrete mutator and cancer phenotypes in mice. *Proceedings of the National Academy of Sciences*, *106*(40), 17101–17104. https://doi.org/10.1073/pnas.0907147106

Al-Hity, G., Yang, F., Campillo-Funollet, E., Greenstein, A. E., Hunt, H., Mampay, M., Intabli, H., Falcinelli, M., Madzvamuse, A., Venkataraman, C., & Flint, M. S. (2021). An integrated framework for quantifying immune-tumour interactions in a 3D co-culture model. *Communications Biology*, *4*(1), 781. https://doi.org/10.1038/s42003-021-02296-7

Amaral, M. V. S., DE SOUSA PORTILHO, A. J., DA SILVA, E. L., DE OLIVEIRA SALES, L., DA SILVA MAUÉS, J. H., DE MORAES, M. E. A., & MOREIRA-NUNES, C. A. (2019). Establishment of Drug-resistant Cell Lines as a Model in Experimental Oncology: A Review. *Anticancer Research*, *39*(12), 6443–6455. https://doi.org/10.21873/anticanres.13858

Amiri, K. I., & Richmond, A. (2005). Role of nuclear factor-κ B in melanoma. *Cancer and Metastasis Reviews*, *24*(2), 301–313. https://doi.org/10.1007/s10555-005-1579-7

Antonello, P., Pizzagalli, D. U., Foglierini, M., Melgrati, S., Radice, E., Thelen, S., & Thelen, M. (2023). ACKR3 promotes CXCL12/CXCR4-mediated cell-to-cell-induced lymphoma migration through LTB4 production. *Frontiers in Immunology*, *13*. https://doi.org/10.3389/fimmu.2022.1067885

Beaumont, K. A., Hill, D. S., Daignault, S. M., Lui, G. Y. L., Sharp, D. M., Gabrielli, B., Weninger, W., & Haass, N. K. (2016). Cell Cycle Phase-Specific Drug Resistance as an Escape Mechanism of Melanoma Cells. *Journal of Investigative Dermatology*, *136*(7), 1479–1489. https://doi.org/10.1016/j.jid.2016.02.805

Benjamini, Y., Drai, D., Elmer, G., Kafkafi, N., & Golani, I. (2001). Controlling the false discovery rate in behavior genetics research. *Behavioural Brain Research*, *125*(1–2), 279–284. https://doi.org/10.1016/S0166-4328(01)00297-2

Benjamini, Y., & Yekutieli, D. (2001). The control of the false discovery rate in multiple testing under dependency. *The Annals of Statistics*, *29*(4). https://doi.org/10.1214/aos/1013699998

Berx, G., & van Roy, F. (2009). Involvement of Members of the Cadherin Superfamily in Cancer. *Cold Spring Harbor Perspectives in Biology*, *1*(6), a003129–a003129. https://doi.org/10.1101/cshperspect.a003129

Bradford, M. (1976). A Rapid and Sensitive Method for the Quantitation of Microgram Quantities of Protein Utilizing the Principle of Protein-Dye Binding. *Analytical Biochemistry*, *72*(1–2), 248–254. https://doi.org/10.1006/abio.1976.9999

Branzei, D., & Foiani, M. (2008). Regulation of DNA repair throughout the cell cycle. *Nature Reviews Molecular Cell Biology*, *9*(4), 297–308. https://doi.org/10.1038/nrm2351

Carlsson, J., & Yuhas, J. M. (1984). *Liquid-Overlay Culture of Cellular Spheroids* (pp. 1–23). https://doi.org/10.1007/978-3-642-82340-4_1

Castedo, M., Perfettini, J.-L., Roumier, T., Andreau, K., Medema, R., & Kroemer, G. (2004). Cell death by mitotic catastrophe: a molecular definition. *Oncogene*, *23*(16), 2825–2837. https://doi.org/10.1038/sj.onc.1207528

Chae, Y. K., Anker, J. F., Oh, M. S., Bais, P., Namburi, S., Agte, S., Giles, F. J., & Chuang, J. H. (2019). Mutations in DNA repair genes are associated with increased neoantigen burden and a distinct immunophenotype in lung squamous cell carcinoma. *Scientific Reports*, *9*(1), 3235. https://doi.org/10.1038/s41598-019-39594-4

Chen, H. F., Ma, R. R., He, J. Y., Zhang, H., Liu, X. L., Guo, X. Y., & Gao, P. (2017). Protocadherin 7 inhibits cell migration and invasion through E-cadherin in gastric cancer. *Tumor Biology*, *39*(4). https://doi.org/10.1177/1010428317697551

Chen, N.-N., Ma, X.-D., Miao, Z., Zhang, X.-M., Han, B.-Y., Almaamari, A. A., Huang, J.-M., Chen, X.-Y., Liu, Y.-J., & Su, S.-W. (2023). Doxorubicin resistance in breast cancer is mediated via the activation of FABP5/PPARγ and CaMKII signaling pathway. *Frontiers in Pharmacology*, *14*. https://doi.org/10.3389/fphar.2023.1150861

Chen, Q., & Wang, Y. (2020). The application of three-dimensional cell culture in clinical medicine. *Biotechnology Letters*, *42*(11), 2071–2082. https://doi.org/10.1007/s10529-020-03003-y

Chen, W., Wong, C., Vosburgh, E., Levine, A. J., Foran, D. J., & Xu, E. Y. (2014). High-throughput Image Analysis of Tumor Spheroids: A User-friendly Software Application to Measure the Size of Spheroids Automatically and Accurately. *Journal of Visualized Experiments*, *89*. https://doi.org/10.3791/51639

Chern, Y. J., & Tai, I. T. (2020). Adaptive response of resistant cancer cells to chemotherapy. In *Cancer Biology and Medicine* (Vol. 17, Issue 4, pp. 842–863). Cancer Biology and Medicine. https://doi.org/10.20892/j.issn.2095-3941.2020.0005

28

Christowitz, C., Davis, T., Isaacs, A., van Niekerk, G., Hattingh, S., & Engelbrecht, A.-M. (2019). Mechanisms of doxorubicin-induced drug resistance and drug resistant tumour growth in a murine breast tumour model. *BMC Cancer*, *19*(1), 757. https://doi.org/10.1186/s12885-019-5939-z

Costa, E. C., Gaspar, V. M., Coutinho, P., & Correia, I. J. (2014). Optimization of liquid overlay technique to formulate heterogenic 3D co-cultures models. *Biotechnology and Bioengineering*, *111*(8), 1672–1685. https://doi.org/10.1002/bit.25210

Cox, J., & Weinman, S. (2016). Mechanisms of doxorubicin resistance in hepatocellular carcinoma. *Hepatic Oncology*, *3*(1), 57–59. https://doi.org/10.2217/hep.15.41

Deng, C., Lin, Y.-X., Qi, X.-K., He, G.-P., Zhang, Y., Zhang, H.-J., Xu, M., Feng, Q.-S., Bei, J.-X., Zeng, Y.-X., & Feng, L. (2023). Correction: TNFRSF19 Inhibits TGFβ Signaling through Interaction with TGFβ Receptor Type 1 to Promote Tumorigenesis. *Cancer Research*, *83*(7), 1158–1158. https://doi.org/10.1158/0008-5472.CAN-23-0141

Duval, V., Alayrac, P., Silvestre, J.-S., & Levoye, A. (2022). Emerging Roles of the Atypical Chemokine Receptor 3 (ACKR3) in Cardiovascular Diseases. *Frontiers in Endocrinology*, *13*. https://doi.org/10.3389/fendo.2022.906586

Elliott, A. M., & Al-Hajj, M. A. (2009). ABCB8 Mediates Doxorubicin Resistance in Melanoma Cells by Protecting the Mitochondrial Genome. *Molecular Cancer Research*, *7*(1), 79–87. https://doi.org/10.1158/1541-7786.MCR-08-0235

Endo, M., Nakano, M., Kadomatsu, T., Fukuhara, S., Kuroda, H., Mikami, S., Hato, T., Aoi, J., Horiguchi, H., Miyata, K., Odagiri, H., Masuda, T., Harada, M., Horio, H., Hishima, T., Nomori, H., Ito, T., Yamamoto, Y., Minami, T., … Oike, Y. (2012). Tumor Cell–Derived Angiopoietin-like Protein ANGPTL2 Is a Critical Driver of Metastasis. *Cancer Research*, *72*(7), 1784–1794. https://doi.org/10.1158/0008-5472.CAN-11-3878

Esposito, I., Kleeff, J., Abiatari, I., Shi, X., Giese, N., Bergmann, F., Roth, W., Friess, H., & Schirmacher, P. (2007). Overexpression of cellular inhibitor of apoptosis protein 2 is an early event in the progression of pancreatic cancer. *Journal of Clinical Pathology*, *60*(8), 885–895. https://doi.org/10.1136/jcp.2006.038257

Fey, S. J., Korzeniowska, B., & Wrzesinski, K. (2020a). Response to and recovery from treatment in human liver-mimetic clinostat spheroids: a model for assessing repeated-dose drug toxicity. *Toxicology Research*, *9*(4), 379–389. https://doi.org/10.1093/toxres/tfaa033

Fey, S. J., Korzeniowska, B., & Wrzesinski, K. (2020b). Response to and recovery from treatment in human liver-mimetic clinostat spheroids: a model for assessing repeated-dose drug toxicity. *Toxicology Research*, *9*(4), 379–389. https://doi.org/10.1093/toxres/tfaa033

Filipiak-Duliban, A., Brodaczewska, K., Kajdasz, A., & Kieda, C. (2022). Spheroid Culture Differentially Affects Cancer Cell Sensitivity to Drugs in Melanoma and RCC Models. *International Journal of Molecular Sciences*, *23*(3). https://doi.org/10.3390/ijms23031166

Friedrich, J., Eder, W., Castaneda, J., Doss, M., Huber, E., Ebner, R., & Kunz-Schughart, L. A. (2007). A Reliable Tool to Determine Cell Viability in Complex 3-D Culture: The Acid Phosphatase Assay. *SLAS Discovery*, *12*(7), 925–937. https://doi.org/10.1177/1087057107306839

Godwin, P., Baird, A. M., Heavey, S., Barr, M. P., O'Byrne, K. J., & Gately, K. (2013). Targeting nuclear factor-kappa B to overcome resistance to chemotherapy. In *Frontiers in Oncology: Vol. 3 MAY*. https://doi.org/10.3389/fonc.2013.00120

Gonzalez-Fernandez, T., Tenorio, A. J., Saiz Jr, A. M., & Leach, J. K. (2022). Engineered Cell-Secreted Extracellular Matrix Modulates Cell Spheroid Mechanosensing and Amplifies Their Response to Inductive Cues for the Formation of Mineralized Tissues. *Advanced Healthcare Materials*, *11*(10). https://doi.org/10.1002/adhm.202102337

Gordon, E., Ravicz, J., Liu, S., Chawla, S., & Hall, F. (2018). Cell cycle checkpoint control: The cyclin G1/Mdm2/p53 axis emerges as a strategic target for broad-spectrum cancer gene therapy - A review of molecular mechanisms for oncologists. *Molecular and Clinical Oncology*. https://doi.org/10.3892/mco.2018.1657

Guan, Y., Du, Y., Wang, G., Gou, H., Xue, Y., Xu, J., Li, E., Chan, D. W., Wu, D., Xu, P., Ni, P., Xu, D., & Hu, Y. (2021). Overexpression of PLXDC2 in Stromal Cell-Associated M2 Macrophages Is Related to EMT and the Progression of Gastric Cancer. *Frontiers in Cell and Developmental Biology*, *9*. https://doi.org/10.3389/fcell.2021.673295

Guo, Y., Zhou, Q., Wei, M., Fan, J., & Huang, H. (2024). Association of TNFRSF19 with a TNF family-based prognostic model and subtypes in gliomas using machine learning. *Heliyon*, *10*(7), e28445. https://doi.org/10.1016/j.heliyon.2024.e28445

Henriet, P., & Emonard, H. (2019). Matrix metalloproteinase-2: Not (just) a “hero” of the past. In *Biochimie* (Vol. 166, pp. 223–232). Elsevier B.V. https://doi.org/10.1016/j.biochi.2019.07.019

Huang, D. W., Sherman, B. T., & Lempicki, R. A. (2009). Systematic and integrative analysis of large gene lists using DAVID bioinformatics resources. *Nature Protocols*, *4*(1), 44–57. https://doi.org/10.1038/nprot.2008.211

Huang, S., Pettaway, C. A., Uehara, H., Bucana, C. D., & Fidler, I. J. (2001). Blockade of NF-κB activity in human prostate cancer cells is associated with suppression of angiogenesis, invasion, and metastasis. *Oncogene*, *20*(31), 4188–4197. https://doi.org/10.1038/sj.onc.1204535

Januchowski, R., Sterzyńska, K., Zaorska, K., Sosińska, P., Klejewski, A., Brązert, M., Nowicki, M., & Zabel, M. (2016). Analysis of MDR genes expression and cross-resistance in eight drug resistant ovarian cancer cell lines. *Journal of Ovarian Research*, *9*(1), 65. https://doi.org/10.1186/s13048-016-0278-z

Jensen, M. R., Factor, V. M., Thorgeirsson, S. S., & Thorgeirsson, S. (1998). *Regulation of Cyclin G1 During Murine Hepatic Regeneration Following Dipin-Induced DNA Damage*.

Kadomatsu, T., Endo, M., Miyata, K., & Oike, Y. (2014). Diverse roles of ANGPTL2 in physiology and pathophysiology. *Trends in Endocrinology & Metabolism*, *25*(5), 245–254. https://doi.org/10.1016/j.tem.2014.03.012

Kapałczyńska, M., Kolenda, T., Przybyła, W., Zajączkowska, M., Teresiak, A., Filas, V., Ibbs, M., Bliźniak, R., Łuczewski, Ł., & Lamperska, K. (2016). 2D and 3D cell cultures – a comparison of different types of cancer cell cultures. *Archives of Medical Science*. https://doi.org/10.5114/aoms.2016.63743

Karthikeyan, M. C., Srinivasan, C., Prabhakar, K., Manogar, P., Jayaprakash, A., & Arockiam, A. J. V. (2024). Doxorubicin downregulates cell cycle regulatory hub genes in breast cancer cells. *Medical Oncology*, *41*(9), 220. https://doi.org/10.1007/s12032-024-02468-5

Kaufmann, W. K., Nevis, K. R., Qu, P., Ibrahim, J. G., Zhou, T., Zhou, Y., Simpson, D. A., Helms-Deaton, J., Cordeiro-Stone, M., Moore, D. T., Thomas, N. E., Hao, H., Liu, Z., Shields, J. M., Scott, G. A., & Sharpless, N. E. (2008). Defective Cell Cycle Checkpoint Functions in Melanoma Are Associated with Altered Patterns of Gene Expression. *Journal of Investigative Dermatology*, *128*(1), 175–187. https://doi.org/10.1038/sj.jid.5700935

Kavanagh, E., Rodhe, J., Burguillos, M. A., Venero, J. L., & Joseph, B. (2014). Regulation of caspase-3 processing by cIAP2 controls the switch between pro-inflammatory activation and cell death in microglia. *Cell Death & Disease*, *5*(12), e1565–e1565. https://doi.org/10.1038/cddis.2014.514

Keijzers, G., Bakula, D., Petr, M. A., Madsen, N. G. K., Teklu, A., Mkrtchyan, G., Osborne, B., & Scheibye-Knudsen, M. (2018). Human Exonuclease 1 (EXO1) Regulatory Functions in DNA Replication with Putative Roles in Cancer. *International Journal of Molecular Sciences*, *20*(1), 74. https://doi.org/10.3390/ijms20010074

Khan, S. U., Fatima, K., Aisha, S., & Malik, F. (2024). Unveiling the mechanisms and challenges of cancer drug resistance. *Cell Communication and Signaling*, *22*(1), 109. https://doi.org/10.1186/s12964-023-01302-1

Kimura, S. H., Ikawa, M., Ito, A., Okabe, M., & Nojima, H. (2001). *Cyclin G1 is involved in G2/M arrest in response to DNA damage and in growth control after damage recovery*. www.nature.com/onc

Kimura, S. H., & Nojima, H. (2002). Cyclin G1 associates with MDM2 and regulates accumulation and degradation of p53 protein. *Genes to Cells*, *7*(8), 869–880. https://doi.org/10.1046/j.1365-2443.2002.00564.x

Kolberg, L., Raudvere, U., Kuzmin, I., Adler, P., Vilo, J., & Peterson, H. (2023). g:Profiler—interoperable web service for functional enrichment analysis and gene identifier mapping (2023 update). *Nucleic Acids Research*, *51*(W1), W207–W212. https://doi.org/10.1093/nar/gkad347

Kuczynski, E. A., Sargent, D. J., Grothey, A., & Kerbel, R. S. (2013). Drug rechallenge and treatment beyond progression—implications for drug resistance. *Nature Reviews Clinical Oncology*, *10*(10), 571–587. https://doi.org/10.1038/nrclinonc.2013.158

Kunz, P., Sähr, H., Lehner, B., Fischer, C., Seebach, E., & Fellenberg, J. (2016). Elevated ratio of MMP2/MMP9 activity is associated with poor response to chemotherapy in osteosarcoma. *BMC Cancer*, *16*(1), 223. https://doi.org/10.1186/s12885-016-2266-5

Kunz-Schughart, L. A., KREUTZ, M., & KNUECHEL, R. (1998). Multicellular spheroids: a three-dimensional *in vitro* culture system to study tumour biology. *International Journal of Experimental Pathology*, *79*(1), 1–23. https://doi.org/10.1046/j.1365-2613.1998.00051.x

Lamichhane, A., Shahi Thakuri, P., Singh, S., Rafsanjani Nejad, P., Heiss, J., Luker, G. D., & Tavana, H. (2022). Therapeutic Targeting of Cancer Stem Cells Prevents Resistance of Colorectal Cancer Cells to MEK Inhibition. *ACS Pharmacology & Translational Science*, *5*(9), 724–734. https://doi.org/10.1021/acsptsci.1c00257

Lamichhane, A., & Tavana, H. (2024). Three-Dimensional Tumor Models to Study Cancer Stemness-Mediated Drug Resistance. *Cellular and Molecular Bioengineering*, *17*(2), 107–119. https://doi.org/10.1007/s12195-024-00798-y

Lang, L., Chen, F., Li, Y., Shay, C., Yang, F., Dan, H., Chen, Z. G., Saba, N. F., & Teng, Y. (2023). Adaptive c-Met-PLXDC2 Signaling Axis Mediates Cancer Stem Cell Plasticity to Confer Radioresistance-associated Aggressiveness in Head and Neck Cancer. *Cancer Research Communications*, *3*(4), 659–671. https://doi.org/10.1158/2767-9764.CRC-22-0289

Leo, R., Therachiyil, L., Siveen, S. K., Uddin, S., Kulinski, M., Buddenkotte, J., Steinhoff, M., & Krishnankutty, R. (2019). Protein Expression Profiling Identifies Key Proteins and Pathways Involved in Growth Inhibitory Effects Exerted by Guggulsterone in Human Colorectal Cancer Cells. *Cancers*, *11*(10), 1478. https://doi.org/10.3390/cancers11101478

Li, A.-M., Tian, A.-X., Zhang, R.-X., Ge, J., Sun, X., & Cao, X.-C. (2013). Protocadherin-7 induces bone metastasis of breast cancer. *Biochemical and Biophysical Research Communications*, *436*(3), 486–490. https://doi.org/10.1016/j.bbrc.2013.05.131

Li, H., Liu, P., Li, D., Wang, Z., Ding, Z., Zhou, M., Chen, X., Miao, M., Ding, J., Lin, W., Liu, Y., & Zha, X. (2022). STAT3/miR-130b-3p/MBNL1 feedback loop regulated by mTORC1 signaling promotes angiogenesis and tumor growth. *Journal of Experimental & Clinical Cancer Research*, *41*(1), 297. https://doi.org/10.1186/s13046-022-02513-z

Li, Y., He, X., Zhang, X., Xu, Y., Chen, W., Liu, X., & Xu, X. (2022). RMI2 is a prognostic biomarker and promotes tumor growth in hepatocellular carcinoma. *Clinical and Experimental Medicine*, *22*(2), 229–243. https://doi.org/10.1007/s10238-021-00742-8

Licarete, E., Rauca, V. F., Luput, L., Drotar, D., Stejerean, I., Patras, L., Dume, B., Toma, V. A., Porfire, A., Gherman, C., Sesarman, A., & Banciu, M. (2020). Overcoming Intrinsic Doxorubicin Resistance in Melanoma by Anti-Angiogenic and Anti-Metastatic Effects of Liposomal Prednisolone Phosphate on Tumor Microenvironment. *International Journal of Molecular Sciences*, *21*(8), 2968. https://doi.org/10.3390/ijms21082968

Licarete, E., Rauca, V., Luput, L., Patras, L., Sesarman, A., & Banciu, M. (2019). The prednisolone phosphate‑induced suppression of the angiogenic function of tumor‑associated macrophages enhances the antitumor effects of doxorubicin on B16.F10 murine melanoma cells in�vitro. *Oncology Reports*. https://doi.org/10.3892/or.2019.7346

Liddiard, K., Aston-Evans, A. N., Cleal, K., Hendrickson, E. A., & Baird, D. M. (2022). POLQ suppresses genome instability and alterations in DNA repeat tract lengths. *NAR Cancer*, *4*(3), zcac020. https://doi.org/10.1093/narcan/zcac020

Liu, L. F. (1989). DNA topoisomerase poisons as antitumor drugs. *Annual Review of Biochemistry*, *58*, 351–375. https://doi.org/10.1146/annurev.bi.58.070189.002031

Livak, K. J., & Schmittgen, T. D. (2001). Analysis of Relative Gene Expression Data Using Real-Time Quantitative PCR and the 2−ΔΔCT Method. *Methods*, *25*(4), 402–408. https://doi.org/10.1006/meth.2001.1262

Longati, P., Jia, X., Eimer, J., Wagman, A., Witt, M.-R., Rehnmark, S., Verbeke, C., Toftgård, R., Löhr, M., & Heuchel, R. L. (2013). 3D pancreatic carcinoma spheroids induce a matrix-rich, chemoresistant phenotype offering a better model for drug testing. *BMC Cancer*, *13*(1), 95. https://doi.org/10.1186/1471-2407-13-95

Lovitt, C. J., Shelper, T. B., & Avery, V. M. (2018). Doxorubicin resistance in breast cancer cells is mediated by extracellular matrix proteins. *BMC Cancer*, *18*(1), 41. https://doi.org/10.1186/s12885-017-3953-6

Luput, L., Licarete, E., Drotar, D. M., Nagy, A.-L., Sesarman, A., Patras, L., Rauca, V. F., Porfire, A., Muntean, D., Achim, M., Tomuta, I., Vlase, L., Catoi, C., Dragos, N., & Banciu, M. (2018). *In Vivo* Double Targeting of C26 Colon Carcinoma Cells and Microenvironmental Protumor Processes Using Liposomal Simvastatin. *Journal of Cancer*, *9*(2), 440–449. https://doi.org/10.7150/jca.21560

Mantovani, A., Barajon, I., & Garlanda, C. (2018). IL-1 and IL-1 regulatory pathways in cancer progression and therapy. *Immunological Reviews*, *281*(1), 57–61. https://doi.org/10.1111/imr.12614

Masuda, T., Endo, M., Yamamoto, Y., Odagiri, H., Kadomatsu, T., Nakamura, T., Tanoue, H., Ito, H., Yugami, M., Miyata, K., Morinaga, J., Horiguchi, H., Motokawa, I., Terada, K., Morioka, M. S., Manabe, I., Iwase, H., Mizuta, H., & Oike, Y. (2015). ANGPTL2 increases bone metastasis of breast cancer cells through enhancing CXCR4 signaling. *Scientific Reports*, *5*(1), 9170. https://doi.org/10.1038/srep09170

Matt, S., & Hofmann, T. G. (2016). The DNA damage-induced cell death response: a roadmap to kill cancer cells. In *Cellular and Molecular Life Sciences* (Vol. 73, Issue 15, pp. 2829–2850). Birkhauser Verlag AG. https://doi.org/10.1007/s00018-016-2130-4

McDermott, M., Eustace, A. J., Busschots, S., Breen, L., Crown, J., Clynes, M., Oâ€™Donovan, N., & Stordal, B. (2014). In vitro Development of Chemotherapy and Targeted Therapy Drug-Resistant Cancer Cell Lines: A Practical Guide with Case Studies. *Frontiers in Oncology*, *4*. https://doi.org/10.3389/fonc.2014.00040

Meguenani, M., Miljkovic-Licina, M., Fagiani, E., Ropraz, P., Hammel, P., Aurrand-Lions, M., Adams, R. H., Christofori, G., Imhof, B. A., & Garrido-Urbani, S. (2015). Junctional adhesion molecule B interferes with angiogenic VEGF/VEGFR2 signaling. *The FASEB Journal*, *29*(8), 3411–3425. https://doi.org/10.1096/fj.15-270223

Melnikova, V. O., Bolshakov, S. V, Walker, C., & Ananthaswamy, H. N. (2004). Genomic alterations in spontaneous and carcinogen-induced murine melanoma cell lines. *Oncogene*, *23*(13), 2347–2356. https://doi.org/10.1038/sj.onc.1207405

Metzger, W., Sossong, D., Bächle, A., Pütz, N., Wennemuth, G., Pohlemann, T., & Oberringer, M. (2011). The liquid overlay technique is the key to formation of co-culture spheroids consisting of primary osteoblasts, fibroblasts and endothelial cells. *Cytotherapy*, *13*(8), 1000–1012. https://doi.org/10.3109/14653249.2011.583233

Meylan, E., Dooley, A. L., Feldser, D. M., Shen, L., Turk, E., Ouyang, C., & Jacks, T. (2009). Requirement for NF-B signalling in a mouse model of lung adenocarcinoma. *Nature*, *462*(7269), 104–107. https://doi.org/10.1038/nature08462

Micheau, O., & Tschopp, J. (2003). Induction of TNF Receptor I-Mediated Apoptosis via Two Sequential Signaling Complexes of these receptors delivers a powerful and rapid proapo-ptotic signal through a DD-mediated recruitment of the adaptor protein FADD and the formation of the so-called complex I fails to induce the expression of antiapoptotic. In *Cell* (Vol. 114).

Mootha, V. K., Lindgren, C. M., Eriksson, K.-F., Subramanian, A., Sihag, S., Lehar, J., Puigserver, P., Carlsson, E., Ridderstråle, M., Laurila, E., Houstis, N., Daly, M. J., Patterson, N., Mesirov, J. P., Golub, T. R., Tamayo, P., Spiegelman, B., Lander, E. S., Hirschhorn, J. N., … Groop, L. C. (2003). PGC-1α-responsive genes involved in oxidative phosphorylation are coordinately downregulated in human diabetes. *Nature Genetics*, *34*(3), 267–273. https://doi.org/10.1038/ng1180

Mrówczyńska, E., Mazurkiewicz, E., & Mazur, A. J. (2022). Gelatin Zymography to Detect Gelatinase Activity in Melanoma Cells. *Journal of Visualized Experiments*, *181*. https://doi.org/10.3791/63278

Mukai, S., Oue, N., Oshima, T., Imai, T., Sekino, Y., Honma, R., Sakamoto, N., Sentani, K., Kuniyasu, H., Egi, H., Tanabe, K., Yoshida, K., Ohdan, H., & Yasui, W. (2017). Overexpression of *PCDHB9* promotes peritoneal metastasis and correlates with poor prognosis in patients with gastric cancer. *The Journal of Pathology*, *243*(1), 100–110. https://doi.org/10.1002/path.4931

Negrea, G., Balacescu, L., Pavel, O., Rauca, V., Dume, B., Licarete Emilia, Patras Laura, & Banciu, M. (2025). Exploring Mechanisms of Early Acquired Resistance to Doxorubicin in Melanoma in 3D Model. *Mendeley Data, V1, Doi: 10.17632/248c3t93fz.1*.

Negrea, G., Rauca, V.-F., Meszaros, M. S., Patras, L., Luput, L., Licarete, E., Toma, V.-A., Porfire, A., Muntean, D., Sesarman, A., & Banciu, M. (2022). Active Tumor-Targeting Nano-formulations Containing Simvastatin and Doxorubicin Inhibit Melanoma Growth and Angiogenesis. *Frontiers in Pharmacology*, *13*. https://doi.org/10.3389/fphar.2022.870347

Nitiss, J. L. (2009). Targeting DNA topoisomerase II in cancer chemotherapy. *Nature Reviews. Cancer*, *9*(5), 338–350. https://doi.org/10.1038/nrc2607

Noort, A. R., van Zoest, K. P., Weijers, E. M., Koolwijk, P., Maracle, C. X., Novack, D. V, Siemerink, M. J., Schlingemann, R. O., Tak, P. P., & Tas, S. W. (2014). NF-κB -inducing kinase is a key regulator of inflammation-induced and tumour-associated angiogenesis. *The Journal of Pathology*, *234*(3), 375–385. https://doi.org/10.1002/path.4403

Okamoto, K., & Beach1, D. (1994). Cyclin G is a transcriptional target of the p53 tumor suppressor protein. In *The EMBO Journal* (Vol. 13, Issue 19).

Okamoto, K., Kamibayashi, † Craig, Serrano, M., Prives, C., Mumby, M. C., & Beach, D. (1996). p53-Dependent Association between Cyclin G and the B Subunit of Protein Phosphatase 2A. In *MOLECULAR AND CELLULAR BIOLOGY* (Vol. 16, Issue 11). http://mcb.asm.org/

Osrodek, M., & Wozniak, M. (2021). Targeting Genome Stability in Melanoma—A New Approach to an Old Field. *International Journal of Molecular Sciences*, *22*(7), 3485. https://doi.org/10.3390/ijms22073485

Pampaloni, F., Reynaud, E. G., & Stelzer, E. H. K. (2007). The third dimension bridges the gap between cell culture and live tissue. *Nature Reviews Molecular Cell Biology*, *8*(10), 839–845. https://doi.org/10.1038/nrm2236

Panneerselvam, M., Bredehorst, R., & Vogel, C. W. (1987). Resistance of human melanoma cells against the cytotoxic and complement-enhancing activities of doxorubicin. *Cancer Research*, *47*(17), 4601–4607.

Paulino, V. M., Yang, Z., Kloss, J., Ennis, M. J., Armstrong, B. A., Loftus, J. C., & Tran, N. L. (2010). TROY (TNFRSF19) Is Overexpressed in Advanced Glial Tumors and Promotes Glioblastoma Cell Invasion via Pyk2-

Rac1 Signaling. *Molecular Cancer Research*, *8*(11), 1558–1567. https://doi.org/10.1158/1541-7786.MCR-10-0334

Pertea, M., Kim, D., Pertea, G. M., Leek, J. T., & Salzberg, S. L. (2016). Transcript-level expression analysis of RNA-seq experiments with HISAT, StringTie and Ballgown. *Nature Protocols*, *11*(9), 1650–1667. https://doi.org/10.1038/nprot.2016.095

Pertea, M., Pertea, G. M., Antonescu, C. M., Chang, T.-C., Mendell, J. T., & Salzberg, S. L. (2015). StringTie enables improved reconstruction of a transcriptome from RNA-seq reads. *Nature Biotechnology*, *33*(3), 290–295. https://doi.org/10.1038/nbt.3122

Pflug, K. M., Lee, D. W., McFadden, K., Herrera, L., & Sitcheran, R. (2023). Transcriptional induction of NF-κB-inducing kinase by E2F4/5 facilitates collective invasion of GBM cells. *Scientific Reports*, *13*(1), 13093. https://doi.org/10.1038/s41598-023-38996-9

Qian, X. Q., Tang, S. S., Shen, Y. M., Chen, L. L., Cheng, X. D., & Wan, X. Y. (2020). Notch1 affects chemo-resistance through regulating epithelial-mesenchymal transition (EMT) in epithelial ovarian cancer cells. *International Journal of Medical Sciences*, *17*(9), 1215–1223. https://doi.org/10.7150/ijms.44683

Rambow, F., Marine, J.-C., & Goding, C. R. (2019). Melanoma plasticity and phenotypic diversity: therapeutic barriers and opportunities. *Genes & Development*, *33*(19–20), 1295–1318. https://doi.org/10.1101/gad.329771.119

Rauca, V.-F., Licarete, E., Luput, L., Sesarman, A., Patras, L., Bulzu, P., Rakosy-Tican, E., & Banciu, M. (2018). Combination therapy of simvastatin and 5, 6-dimethylxanthenone-4-acetic acid synergistically suppresses the aggressiveness of B16.F10 melanoma cells. *PLOS ONE*, *13*(8), e0202827. https://doi.org/10.1371/journal.pone.0202827

Raudvere, U., Kolberg, L., Kuzmin, I., Arak, T., Adler, P., Peterson, H., & Vilo, J. (2019). g:Profiler: a web server for functional enrichment analysis and conversions of gene lists (2019 update). *Nucleic Acids Research*, *47*(W1), W191–W198. https://doi.org/10.1093/nar/gkz369

Rezayatmand, H., Razmkhah, M., & Razeghian-Jahromi, I. (2022). Drug resistance in cancer therapy: the Pandora's Box of cancer stem cells. *Stem Cell Research & Therapy*, *13*(1), 181. https://doi.org/10.1186/s13287-022-02856-6

Robinson, M. D., McCarthy, D. J., & Smyth, G. K. (2010). <tt>edgeR</tt> : a Bioconductor package for differential expression analysis of digital gene expression data. *Bioinformatics*, *26*(1), 139–140. https://doi.org/10.1093/bioinformatics/btp616

Ryl, T., Kuchen, E. E., Bell, E., Shao, C., Flórez, A. F., Mönke, G., Gogolin, S., Friedrich, M., Lamprecht, F., Westermann, F., & Höfer, T. (2017). Cell-Cycle Position of Single MYC-Driven Cancer Cells Dictates Their Susceptibility to a Chemotherapeutic Drug. *Cell Systems*, *5*(3), 237-250.e8. https://doi.org/10.1016/j.cels.2017.07.005

Sertic, S., Pizzi, S., Cloney, R., Lehmann, A. R., Marini, F., Plevani, P., & Muzi-Falconi, M. (2011). Human exonuclease 1 connects nucleotide excision repair (NER) processing with checkpoint activation in response to UV irradiation. *Proceedings of the National Academy of Sciences*, *108*(33), 13647–13652. https://doi.org/10.1073/pnas.1108547108

Sezer, E. D., Oktay, L. M., Karadadaş, E., Memmedov, H., Selvi Gunel, N., & Sözmen, E. (2019). Assessing Anticancer Potential of Blueberry Flavonoids, Quercetin, Kaempferol, and Gentisic Acid, Through Oxidative Stress and Apoptosis Parameters on HCT-116 Cells. *Journal of Medicinal Food*, *22*(11), 1118–1126. https://doi.org/10.1089/jmf.2019.0098

Shahi Thakuri, P., Luker, G. D., & Tavana, H. (2019). Cyclical Treatment of Colorectal Tumor Spheroids Induces Resistance to MEK Inhibitors. *Translational Oncology*, *12*(3), 404–416. https://doi.org/10.1016/j.tranon.2018.11.009

Sherman, B. T., Hao, M., Qiu, J., Jiao, X., Baseler, M. W., Lane, H. C., Imamichi, T., & Chang, W. (2022). DAVID: a web server for functional enrichment analysis and functional annotation of gene lists (2021 update). *Nucleic Acids Research*, *50*(W1), W216–W221. https://doi.org/10.1093/nar/gkac194

Singh, T. R., Ali, A. M., Busygina, V., Raynard, S., Fan, Q., Du, C. H., Andreassen, P. R., Sung, P., & Meetei, A. R. (2008). BLAP18/RMI2, a novel OB-fold-containing protein, is an essential component of the Bloom helicase-double Holliday junction dissolvasome. *Genes and Development*, *22*(20), 2856–2868. https://doi.org/10.1101/gad.1725108

Singvogel, K., & Schittek, B. (2024). Dormancy of cutaneous melanoma. *Cancer Cell International*, *24*(1), 88. https://doi.org/10.1186/s12935-024-03278-5

Smith, J. C., & Sheltzer, J. M. (2022). Genome-wide identification and analysis of prognostic features in human cancers. *Cell Reports*, *38*(13), 110569. https://doi.org/10.1016/j.celrep.2022.110569

Smith, L., Watson, M. B., O'Kane, S. L., Drew, P. J., Lind, M. J., & Cawkwell, L. (2006). The analysis of doxorubicin resistance in human breast cancer cells using antibody microarrays. *Molecular Cancer Therapeutics*, *5*(8), 2115–2120. https://doi.org/10.1158/1535-7163.MCT-06-0190

Spallarossa, P., ALTIERI, P., GARIBALDI, S., GHIGLIOTTI, G., BARISIONE, C., MANCA, V., FABBI, P., BALLESTRERO, A., BRUNELLI, C., & BARSOTTI, A. (2006). Matrix metalloproteinase-2 and -9 are induced differently by doxorubicin in H9c2 cells: The role of MAP kinases and NAD(P)H oxidase. *Cardiovascular Research*, *69*(3), 736–745. https://doi.org/10.1016/j.cardiores.2005.08.009

Srinivasan, B., & Lloyd, M. D. (2024). Dose–Response Curves and the Determination of IC $_{50}$ and EC $_{50}$ Values. *Journal of Medicinal Chemistry*, *67*(20), 17931–17934. https://doi.org/10.1021/acs.jmedchem.4c02052

Subramanian, A., Tamayo, P., Mootha, V. K., Mukherjee, S., Ebert, B. L., Gillette, M. A., Paulovich, A., Pomeroy, S. L., Golub, T. R., Lander, E. S., & Mesirov, J. P. (2005). Gene set enrichment analysis: A knowledge-based approach for interpreting genome-wide expression profiles. *Proceedings of the National Academy of Sciences*, *102*(43), 15545–15550. https://doi.org/10.1073/pnas.0506580102

Taylor, S. C., Berkelman, T., Yadav, G., & Hammond, M. (2013). A Defined Methodology for Reliable Quantification of Western Blot Data. *Molecular Biotechnology*, *55*(3), 217–226. https://doi.org/10.1007/s12033-013-9672-6

Thiem, S., Pierce, T. P., Palmieri, M., Putoczki, T. L., Buchert, M., Preaudet, A., Farid, R. O., Love, C., Catimel, B., Lei, Z., Rozen, S., Gopalakrishnan, V., Schaper, F., Hallek, M., Boussioutas, A., Tan, P., Jarnicki, A., & Ernst, M. (2013). mTORC1 inhibition restricts inflammation-associated gastrointestinal tumorigenesis in mice. *Journal of Clinical Investigation*. https://doi.org/10.1172/JCI65086

Thorn, C. F., Oshiro, C., Marsh, S., Hernandez-Boussard, T., McLeod, H., Klein, T. E., & Altman, R. B. (2011). Doxorubicin pathways: Pharmacodynamics and adverse effects. *Pharmacogenetics and Genomics*, *21*(7), 440–446. https://doi.org/10.1097/FPC.0b013e32833ffb56

Tormo, E., Ballester, S., Adam-Artigues, A., Burgués, O., Alonso, E., Bermejo, B., Menéndez, S., Zazo, S., Madoz-Gúrpide, J., Rovira, A., Albanell, J., Rojo, F., Lluch, A., & Eroles, P. (2019). The miRNA-449 family mediates doxorubicin resistance in triple-negative breast cancer by regulating cell cycle factors. *Scientific Reports*, *9*(1), 5316. https://doi.org/10.1038/s41598-019-41472-y

Toth, M., & Fridman, R. (2001). Assessment of Gelatinases (MMP-2 and MMP-9 by Gelatin Zymography. *Methods in Molecular Medicine*, *57*, 163–174. https://doi.org/10.1385/1-59259-136-1:163

Tune, B. X. J., Sim, M. S., Poh, C. L., Guad, R. Mac, Woon, C. K., Hazarika, I., Das, A., Gopinath, S. C. B., Rajan, M., Sekar, M., Subramaniyan, V., Fuloria, N. K., Fuloria, S., Batumalaie, K., & Wu, Y. S. (2022). Matrix Metalloproteinases in Chemoresistance: Regulatory Roles, Molecular Interactions, and Potential Inhibitors. In *Journal of Oncology* (Vol. 2022). Hindawi Limited. https://doi.org/10.1155/2022/3249766

Vera, J., Raatz, Y., Wolkenhauer, O., Kottek, T., Bhattacharya, A., Simon, J. C., & Kunz, M. (2015). Chk1 and Wee1 control genotoxic-stress induced G2–M arrest in melanoma cells. *Cellular Signalling*, *27*(5), 951–960. https://doi.org/10.1016/j.cellsig.2015.01.020

Visconti, R., Della Monica, R., & Grieco, D. (2016). Cell cycle checkpoint in cancer: a therapeutically targetable double-edged sword. *Journal of Experimental & Clinical Cancer Research*, *35*(1), 153. https://doi.org/10.1186/s13046-016-0433-9

Vorobiof, D. A., Rapoport, B. L., Mahomed, R., & Karime, M. (2003). Phase II study of pegylated liposomal doxorubicin in patients with metastatic malignant melanoma failing standard chemotherapy treatment. *Melanoma Research*, *13*(2), 201–203. https://doi.org/10.1097/00008390-200304000-00015

Wang, J. Y. J. (2019). Cell Death Response to DNA Damage. In *YALE JOURNAL OF BIOLOGY AND MEDICINE* (Vol. 92).

Wang, Q., Lu, F., & Lan, R. (2017). RNA-sequencing dissects the transcriptome of polyploid cancer cells that are resistant to combined treatments of cisplatin with paclitaxel and docetaxel. *Molecular BioSystems*, *13*(10), 2125–2134. https://doi.org/10.1039/C7MB00334J

Wang, Z., Li, Y., Ahmad, A., Azmi, A. S., Banerjee, S., Kong, D., & Sarkar, F. H. (2010). Targeting Notch signaling pathway to overcome drug resistance for cancer therapy. *Biochimica et Biophysica Acta (BBA) - Reviews on Cancer*, *1806*(2), 258–267. https://doi.org/10.1016/j.bbcan.2010.06.001

Weinguny, M., Klanert, G., Eisenhut, P., Jonsson, A., Ivansson, D., Lövgren, A., & Borth, N. (2020). Directed evolution approach to enhance efficiency and speed of outgrowth during single cell subcloning of Chinese Hamster Ovary cells. *Computational and Structural Biotechnology Journal*, *18*, 1320–1329. https://doi.org/10.1016/j.csbj.2020.05.020

Wu, B., Wang, Y., Wang, J., Xiang, D., Zhang, M., Yan, Z., Wang, W., Miao, J., Lan, X., Liu, J., Li, Z., Li, C., Fan, J., Liu, J., Jiang, L., Xu, S., Cui, Y., & Qian, F. (2022). PLXDC2 enhances invadopodium formation to promote invasion and metastasis of gastric cancer cells via interacting with PTP1B. *Clinical & Experimental Metastasis*, *39*(4), 691–710. https://doi.org/10.1007/s10585-022-10168-5

Wu, S., & Singh, R. K. (2011). Resistance to Chemotherapy and Molecularly Targeted Therapies: Rationale for Combination Therapy in Malignant Melanoma. *Current Molecular Medicine*, *11*(7), 553–563. https://doi.org/10.2174/156652411800615153

Wu, Y., & Zhou, B. P. (2010). TNF-α/NF-κB/Snail pathway in cancer cell migration and invasion. *British Journal of Cancer*, *102*(4), 639–644. https://doi.org/10.1038/sj.bjc.6605530

Xia, Y., Shen, S., & Verma, I. M. (2014). NF-κB, an Active Player in Human Cancers. *Cancer Immunology Research*, *2*(9), 823–830. https://doi.org/10.1158/2326-6066.CIR-14-0112

Xiao, D., Dong, S., Yang, S., & Liu, Z. (2020). CKS2 and RMI2 are two prognostic biomarkers of lung adenocarcinoma. *PeerJ*, *8*. https://doi.org/10.7717/peerj.10126

Xie, Y., Liu, Y.-K., Guo, Z.-P., Guan, H., Liu, X.-D., Xie, D.-F., Jiang, Y.-G., Ma, T., & Zhou, P.-K. (2020). RBX1 prompts degradation of EXO1 to limit the homologous recombination pathway of DNA double-strand break repair in G1 phase. *Cell Death & Differentiation*, *27*(4), 1383–1397. https://doi.org/10.1038/s41418-019-0424-4

Zhan, W., Liu, Y., Gao, Y., Gong, R., Wang, W., Zhang, R., Wu, Y., Kang, T., & Wei, D. (2020). RMI2 plays crucial roles in growth and metastasis of lung cancer. In *Signal Transduction and Targeted Therapy* (Vol. 5, Issue 1). Springer Nature. https://doi.org/10.1038/s41392-020-00295-4

Zhang, J. X., Lau, E., Paik, D. T., Zhuge, Y., & Wu, J. C. (2020). High-throughput Preparation of DNA, RNA, and Protein from Cryopreserved Human iPSCs for Multi-omics Analysis. *Current Protocols in Stem Cell Biology*, *54*(1). https://doi.org/10.1002/cpsc.114

Zheng, Z., Luan, N., Tu, K., Liu, F., Wang, J., & Sun, J. (2023). The roles of protocadherin-7 in colorectal cancer cells on cell proliferation and its chemoresistance. *Frontiers in Pharmacology*, *14*. https://doi.org/10.3389/fphar.2023.1072033

Zhu, P., Lv, J., Yang, Z., Guo, L., Zhang, L., Li, M., Han, W., Chen, X., Zhuang, H., & Lu, F. (2014). Protocadherin 9 inhibits epithelial-mesenchymal transition and cell migration through activating GSK-3β in hepatocellular carcinoma. *Biochemical and Biophysical Research Communications*, *452*(3), 567–574. https://doi.org/10.1016/j.bbrc.2014.08.101

35

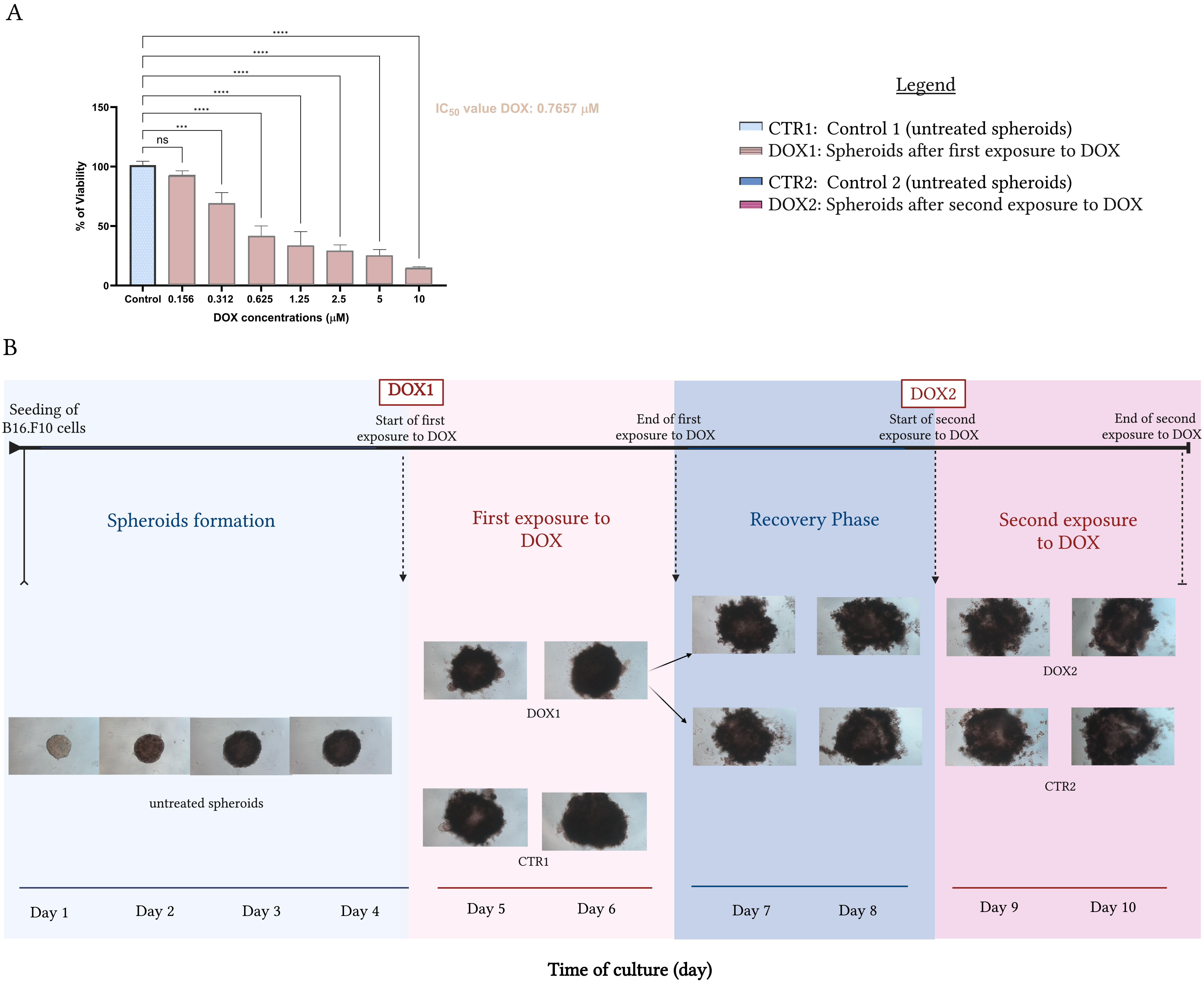
A
% of Viability
150
100
50
0
ns
***
****
****
****
****
****
Control
0.156
0.312
0.625
1.25
2.5
5
10
DOX concentrations (µM)
IC$_{50}$ value DOX: 0.7657 µM
Legend
CTR1: Control 1 (untreated spheroids)
DOX1: Spheroids after first exposure to DOX
CTR2: Control 2 (untreated spheroids)
DOX2: Spheroids after second exposure to DOX
B
Seeding of B16.F10 cells
DOX1
Start of first exposure to DOX
End of first exposure to DOX
DOX2
Start of second exposure to DOX
End of second exposure to DOX
Spheroids formation
First exposure to DOX
Recovery Phase
Second exposure to DOX
DOX1
CTR1
DOX2
CTR2
untreated spheroids
Day 1
Day 2
Day 3
Day 4
Day 5
Day 6
Day 7
Day 8
Day 9
Day 10
Time of culture (day)

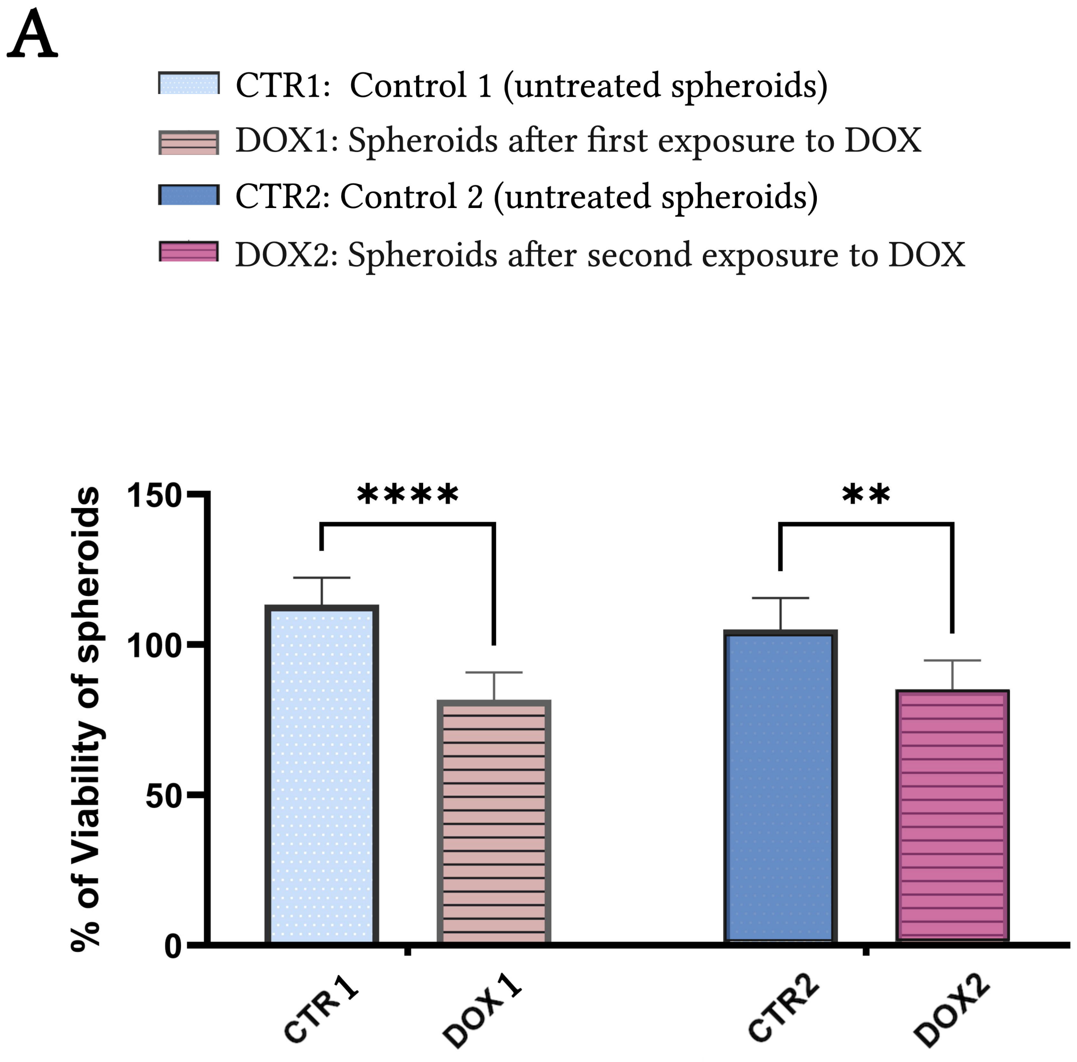

B

DOX treatment	K_{DOX} and K_{CTR} Growth rate average (mm³/day)		K_{DOX}/K_{CTR} Resistance growth marker
	K_{DOX}	K_{CTR}	
First exposure	0.0154 ± 0.006	0.0570 ± 0.011	0.271
Second exposure	0.0015 ± 0.012	0.0153 ± 0.013	0.098

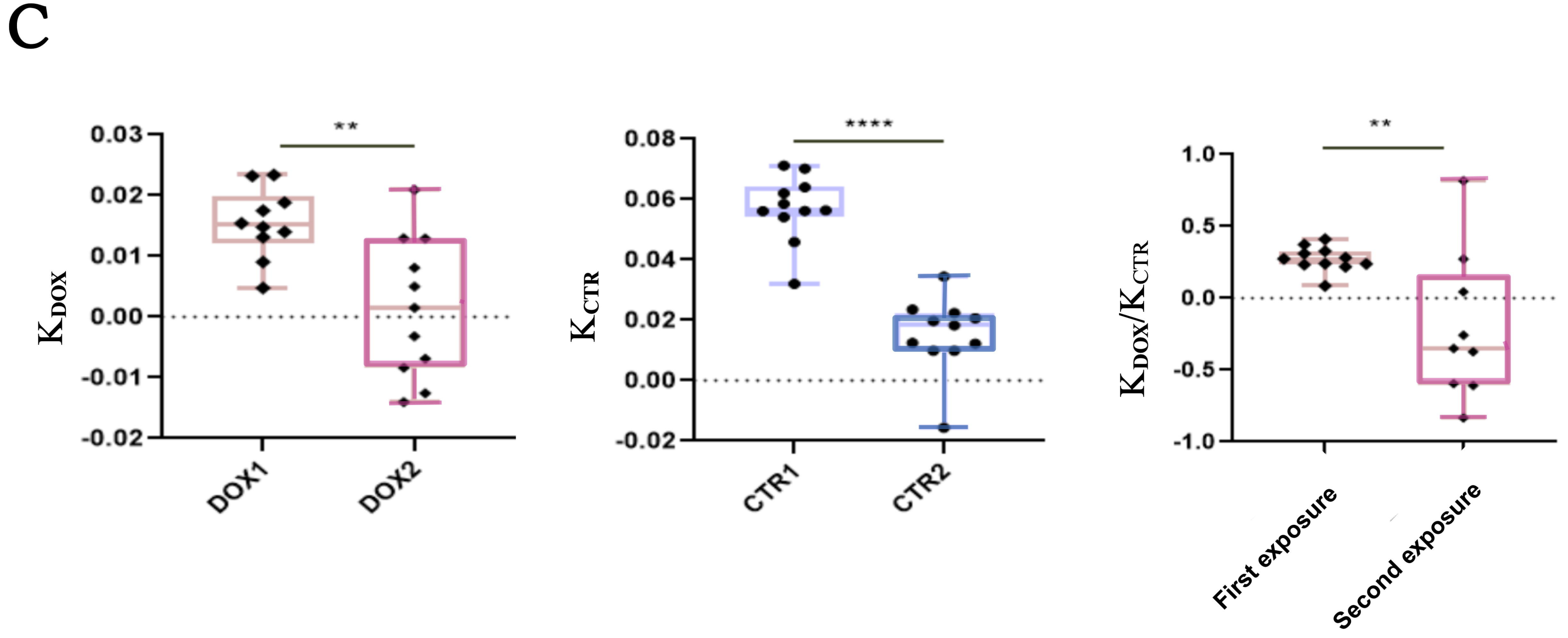

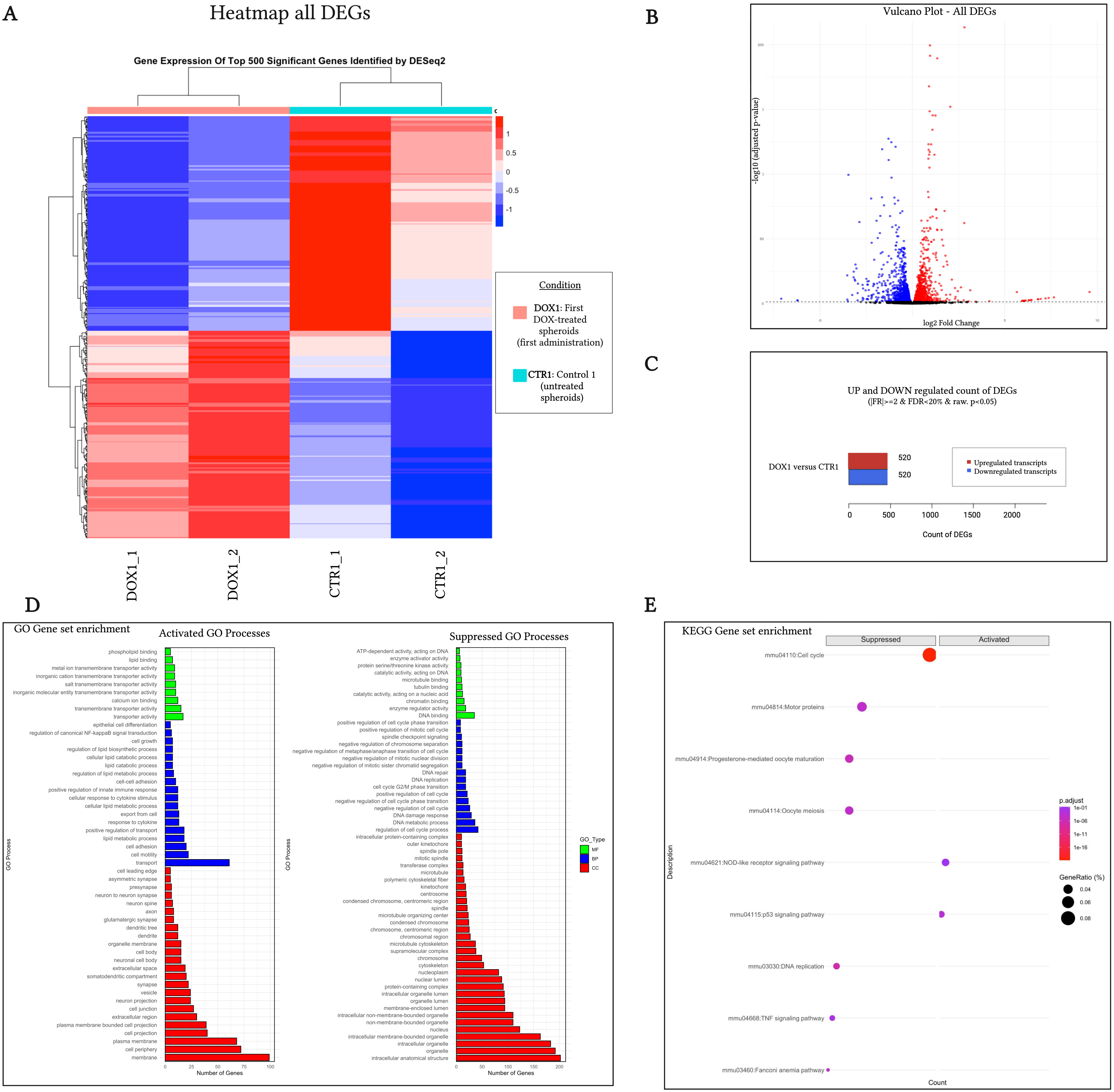
A
Heatmap all DEGs
Gene Expression Of Top 500 Significant Genes Identified by DESeq2
1
0.5
0
-0.5
-1
Condition
DOX1: First DOX-treated spheroids (first administration)
CTR1: Control 1 (untreated spheroids)
DOX1_1
DOX1_2
CTR1_1
CTR1_2
B
Vulcano Plot - All DEGs
-log10 (adjusted p-value)
200
50
0
log2 Fold Change
-5
5
10
C
UP and DOWN regulated count of DEGs
(|FR|>=2 & FDR<20% & raw. p<0.05)
DOX1 versus CTR1
520
520
Upregulated transcripts
Downregulated transcripts
0
500
1000
1500
2000
Count of DEGs
D
GO Gene set enrichment
Activated GO Processes
phospholipid binding
lipid binding
metal ion transmembrane transporter activity
inorganic cation transmembrane transporter activity
salt transmembrane transporter activity
inorganic molecular entity transmembrane transporter activity
calcium ion binding
transmembrane transporter activity
transporter activity
epithelial cell differentiation
regulation of canonical NF-kappaB signal transduction
cell growth
regulation of lipid biosynthetic process
cellular lipid catabolic process
lipid catabolic process
regulation of lipid metabolic process
cell-cell adhesion
positive regulation of innate immune response
cellular response to cytokine stimulus
cellular lipid metabolic process
export from cell
response to cytokine
positive regulation of transport
lipid metabolic process
cell adhesion
cell motility
transport
cell leading edge
asymmetric synapse
presynapse
neuron to neuron synapse
neuron spine
axon
glutamatergic synapse
dendritic tree
dendrite
organelle membrane
cell body
neuronal cell body
extracellular space
somatodendritic compartment
synapse
vesicle
neuron projection
cell junction
extracellular region
plasma membrane bounded cell projection
cell projection
plasma membrane
cell periphery
membrane
GO Process
0
25
50
75
100
Number of Genes
Suppressed GO Processes
ATP-dependent activity, acting on DNA
enzyme activator activity
protein serine/threonine kinase activity
catalytic activity, acting on DNA
microtubule binding
tubulin binding
catalytic activity, acting on a nucleic acid
chromatin binding
enzyme regulator activity
DNA binding
positive regulation of cell cycle phase transition
positive regulation of mitotic cell cycle
spindle checkpoint signaling
negative regulation of chromosome separation
negative regulation of metaphase/anaphase transition of cell cycle
negative regulation of mitotic nuclear division
negative regulation of mitotic sister chromatid segregation
DNA repair
DNA replication
cell cycle G2/M phase transition
positive regulation of cell cycle
negative regulation of cell cycle phase transition
negative regulation of cell cycle
DNA damage response
DNA metabolic process
regulation of cell cycle process
intracellular protein-containing complex
outer kinetochore
spindle pole
mitotic spindle
transferase complex
microtubule
polymeric cytoskeletal fiber
kinetochore
centrosome
condensed chromosome, centromeric region
spindle
microtubule organizing center
condensed chromosome
chromosome, centromeric region
chromosomal region
microtubule cytoskeleton
supramolecular complex
chromosome
cytoskeleton
nucleoplasm
nuclear lumen
protein-containing complex
intracellular organelle lumen
organelle lumen
membrane-enclosed lumen
intracellular non-membrane-bounded organelle
non-membrane-bounded organelle
nucleus
intracellular membrane-bounded organelle
intracellular organelle
organelle
intracellular anatomical structure
GO Process
0
50
100
150
200
Number of Genes
GO_Type
MF
BP
CC
E
KEGG Gene set enrichment
Suppressed
Activated
mmu04110:Cell cycle
mmu04814:Motor proteins
mmu04914:Progesterone-mediated oocyte maturation
mmu04114:Oocyte meiosis
mmu04621:NOD-like receptor signaling pathway
mmu04115:p53 signaling pathway
mmu03030:DNA replication
mmu04668:TNF signaling pathway
mmu03460:Fanconi anemia pathway
Description
Count
p.adjust
1e-01
1e-06
1e-11
1e-16
GeneRatio (%)
0.04
0.06
0.08

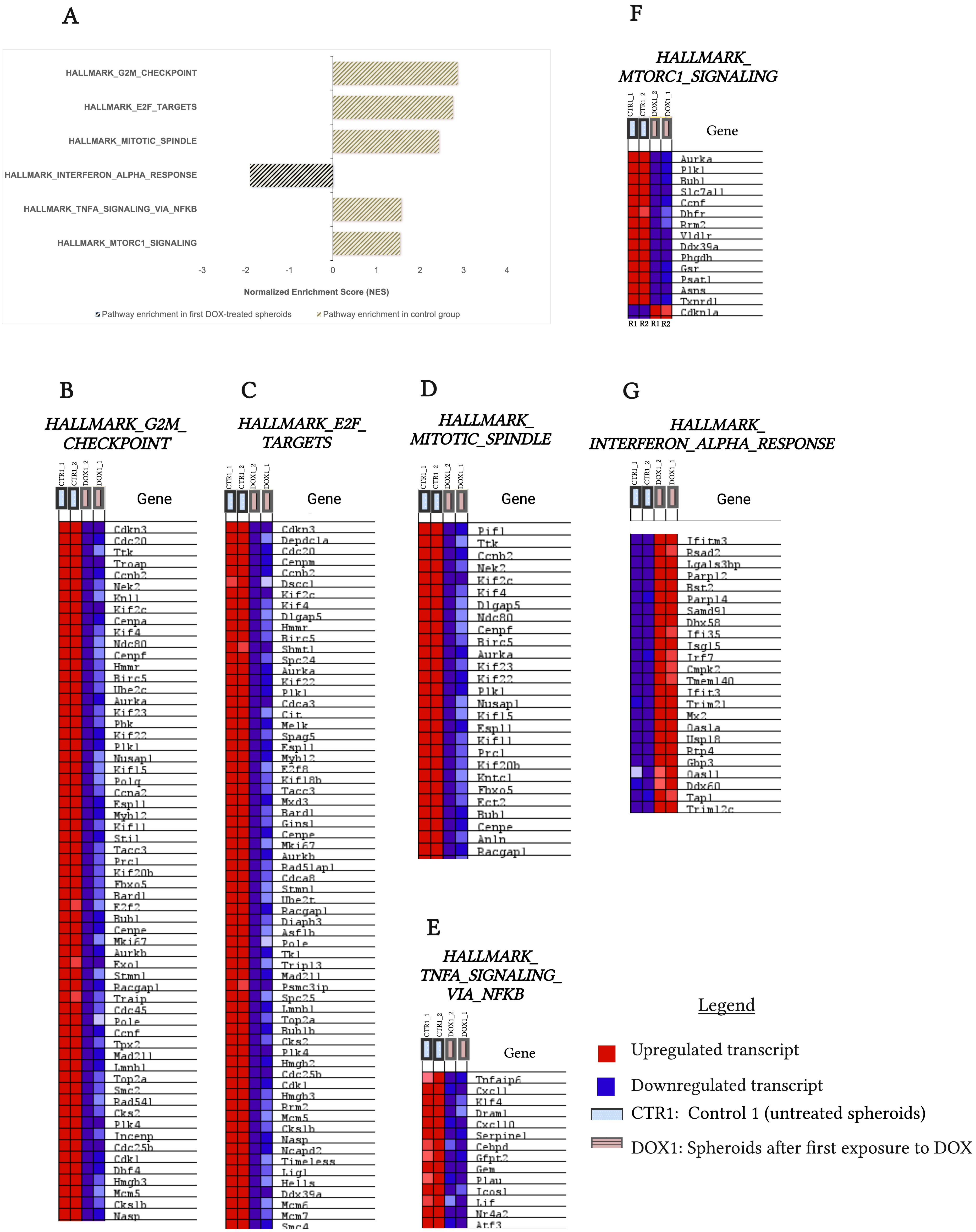
A
HALLMARK_G2M_CHECKPOINT
HALLMARK_E2F_TARGETS
HALLMARK_MITOTIC_SPINDLE
HALLMARK_INTERFERON_ALPHA_RESPONSE
HALLMARK_TNFA_SIGNALING_VIA_NFKB
HALLMARK_MTORC1_SIGNALING
-3
-2
-1
0
1
2
3
4
Normalized Enrichment Score (NES)
Pathway enrichment in first DOX-treated spheroids
Pathway enrichment in control group
F
HALLMARK_
MTORC1_SIGNALING
CTR1_1
CTR1_2
DOX1_2
DOX1_1
Gene
Aurka
Plk1
Bub1
Slc7a11
Ccnf
Dhfr
Rrm2
Vldlr
Ddx39a
Phgdh
Gsr
Psat1
Asns
Txnrd1
Cdkn1a
R1 R2 R1 R2
B
HALLMARK_G2M_
CHECKPOINT
CTR1_1
CTR1_2
DOX1_2
DOX1_1
Gene
Cdkn3
Cdc20
Ttk
Troap
Ccnb2
Nek2
Knl1
Kif2c
Cenpa
Kif4
Ndc80
Cenpf
Hmmr
Birc5
Ube2c
Aurka
Kif23
Pbk
Kif22
Plk1
Nusap1
Kif15
Polq
Ccna2
Espl1
Mybl2
Kif11
Stil
Tacc3
Prc1
Kif20b
Fbxo5
Bard1
E2f2
Bub1
Cenpe
Mki67
Aurkb
Exo1
Stmn1
Racgap1
Traip
Cdc45
Pole
Ccnf
Tpx2
Mad2l1
Lmnb1
Top2a
Smc2
Rad54l
Cks2
Plk4
Incenp
Cdc25b
Cdk1
Dbf4
Hmgb3
Mcm5
Cks1b
Nasp
C
HALLMARK_E2F_
TARGETS
CTR1_1
CTR1_2
DOX1_2
DOX1_1
Gene
Cdkn3
Depdc1a
Cdc20
Cenpm
Ccnb2
Dscc1
Kif2c
Kif4
Dlgap5
Hmmr
Birc5
Shmt1
Spc24
Aurka
Kif22
Plk1
Cdca3
Cit
Melk
Spag5
Espl1
Mybl2
E2f8
Kif18b
Tacc3
Mxd3
Bard1
Gins1
Cenpe
Mki67
Aurkb
Rad51ap1
Cdca8
Stmn1
Ube2t
Racgap1
Diaph3
Asf1b
Pole
Tk1
Trip13
Mad2l1
Psmc3ip
Spc25
Lmnb1
Top2a
Bub1b
Cks2
Plk4
Hmgb2
Cdc25b
Cdk1
Hmgb3
Rrm2
Mcm5
Cks1b
Nasp
Ncapd2
Timeless
Lig1
Hells
Ddx39a
Mcm6
Mcm7
Smc4
D
HALLMARK_
MITOTIC_SPINDLE
CTR1_1
CTR1_2
DOX1_2
DOX1_1
Gene
Pif1
Ttk
Ccnb2
Nek2
Kif2c
Kif4
Dlgap5
Ndc80
Cenpf
Birc5
Aurka
Kif23
Kif22
Plk1
Nusap1
Kif15
Espl1
Kif11
Prc1
Kif20b
Kntc1
Fbxo5
Ect2
Bub1
Cenpe
Anln
Racgap1
G
HALLMARK_
INTERFERON_ALPHA_RESPONSE
CTR1_1
CTR1_2
DOX1_2
DOX1_1
Gene
Ifitm3
Rsad2
Lgals3bp
Parp12
Bst2
Parp14
Samd9l
Dhx58
Ifi35
Isg15
Irf7
Cmpk2
Tmem140
Ifit3
Trim21
Mx2
Oas1a
Usp18
Rtp4
Gbp3
Oasl1
Ddx60
Tap1
Trim12c
E
HALLMARK_
TNFA_SIGNALING_
VIA_NFKB
CTR1_1
CTR1_2
DOX1_2
DOX1_1
Gene
Tnfaip6
Cxcl1
Klf4
Dram1
Cxcl10
Serpine1
Cebpd
Gfpt2
Gem
Plau
Icosl
Lif
Nr4a2
Atf3
Legend
Upregulated transcript
Downregulated transcript
CTR1: Control 1 (untreated spheroids)
DOX1: Spheroids after first exposure to DOX

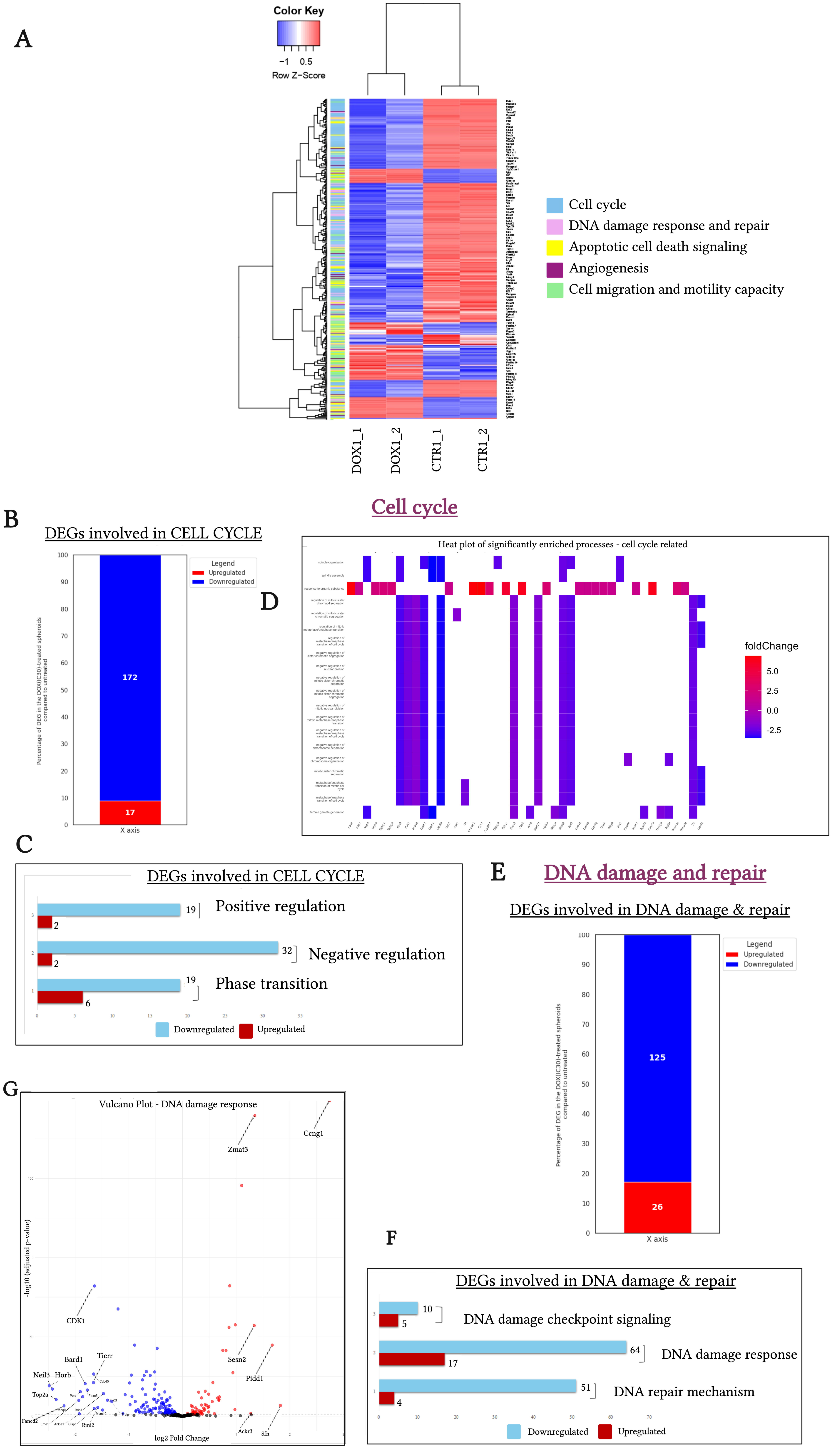A
Color Key
−1 0.5
Row Z−Score
Cell cycle
DNA damage response and repair
Apoptotic cell death signaling
Angiogenesis
Cell migration and motility capacity
DOX1_1
DOX1_2
CTR1_1
CTR1_2
B
DEGs involved in CELL CYCLE
Legend
Upregulated
Downregulated
Percentage of DEG in the DOX(IC30)-treated spheroids compared to untreated
172
17
X axis
Cell cycle
D
Heat plot of significantly enriched processes - cell cycle related
foldChange
5.0
2.5
0.0
-2.5
C
DEGs involved in CELL CYCLE
Positive regulation
Negative regulation
Phase transition
19
2
32
2
19
6
Downregulated
Upregulated
E
DNA damage and repair
DEGs involved in DNA damage & repair
Legend
Upregulated
Downregulated
Percentage of DEG in the DOX(IC30)-treated spheroids compared to untreated
125
26
X axis
G
Vulcano Plot - DNA damage response
-log10 (adjusted p-value)
log2 Fold Change
Ccng1
Zmat3
CDK1
Sesn2
Pidd1
Bard1
Ticrr
Neil3
Horb
Top2a
Fancd2
Rmi2
Ackr3
Sfn
F
DEGs involved in DNA damage & repair
DNA damage checkpoint signaling
DNA damage response
DNA repair mechanism
10
5
64
17
51
4
Downregulated
Upregulated

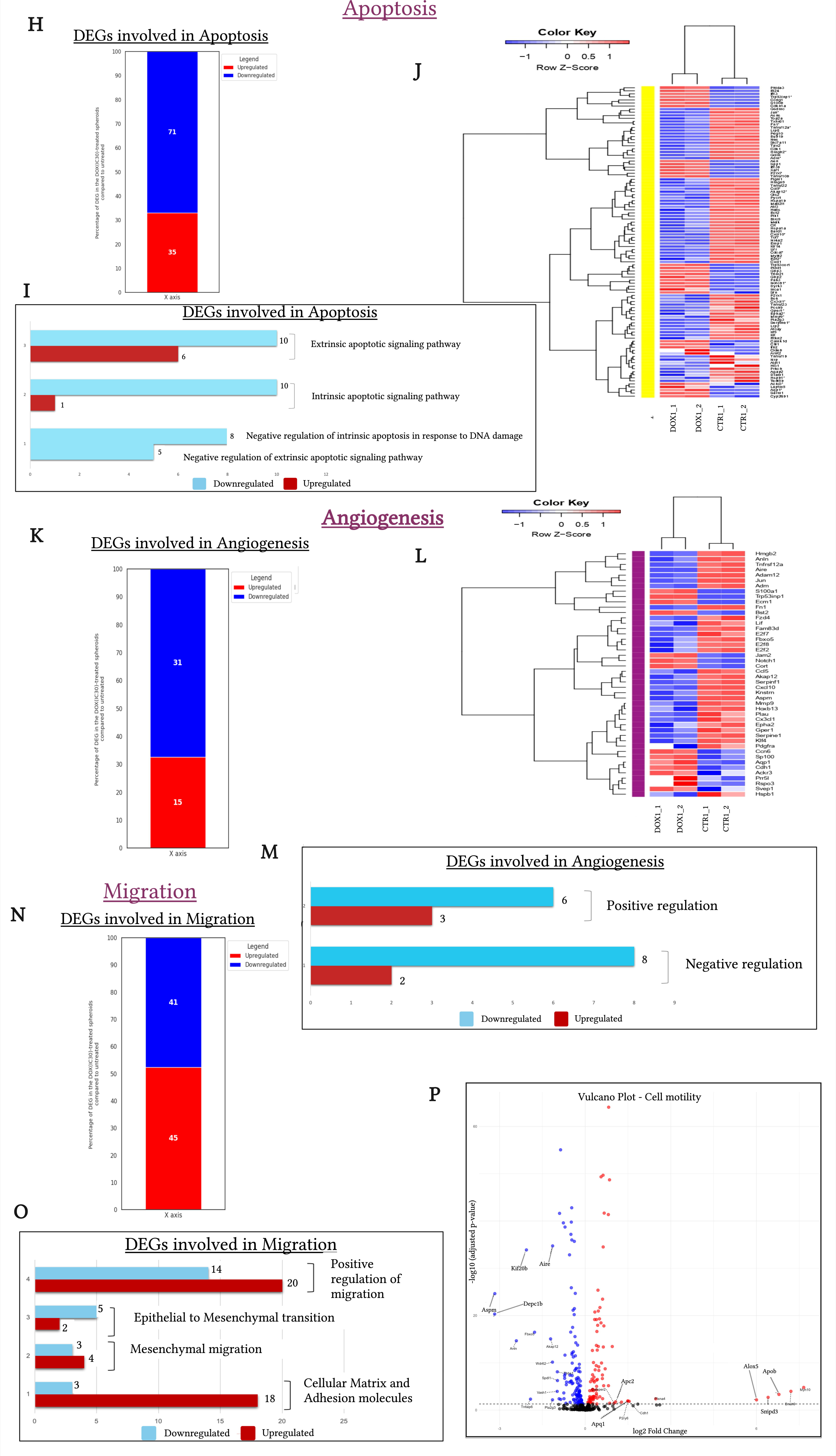
Apoptosis
H
DEGs involved in Apoptosis
Percentage of DEG in the DOX(IC30)-treated spheroids compared to untreated
100
90
80
70
60
50
40
30
20
10
0
71
35
X axis
Legend
Upregulated
Downregulated
J
Color Key
−1
0
0.5
1
Row Z−Score
DOX1_1
DOX1_2
CTR1_1
CTR1_2
I
DEGs involved in Apoptosis
3
2
1
10
6
Extrinsic apoptotic signaling pathway
10
1
Intrinsic apoptotic signaling pathway
8
Negative regulation of intrinsic apoptosis in response to DNA damage
5
Negative regulation of extrinsic apoptotic signaling pathway
0
2
4
6
8
10
12
Downregulated
Upregulated
Angiogenesis
K
DEGs involved in Angiogenesis
Percentage of DEG in the DOX(IC30)-treated spheroids compared to untreated
100
90
80
70
60
50
40
30
20
10
0
31
15
X axis
Legend
Upregulated
Downregulated
L
Color Key
−1
0
0.5
1
Row Z−Score
Hmgb2
Anln
Tnfrsf12a
Aire
Adam12
Jun
Adm
S100a1
Trp53inp1
Ecm1
Fn1
Bst2
Fzd4
Lif
Fam83d
E2f7
Fbxo5
E2f8
E2f2
Jam2
Notch1
Cort
Ccl5
Akap12
Serpinf1
Cxcl10
Knstrn
Aspm
Mmp9
Hoxb13
Plau
Cx3cl1
Epha2
Gper1
Serpine1
Klf4
Pdgfra
Ccn6
Sp100
Aqp1
Cdh1
Ackr3
Prr5l
Rspo3
Svep1
Hspb1
DOX1_1
DOX1_2
CTR1_1
CTR1_2
M
DEGs involved in Angiogenesis
2
1
6
3
Positive regulation
8
2
Negative regulation
0
1
2
3
4
5
6
7
8
9
Downregulated
Upregulated
Migration
N
DEGs involved in Migration
Percentage of DEG in the DOX(IC30)-treated spheroids compared to untreated
100
90
80
70
60
50
40
30
20
10
0
41
45
X axis
Legend
Upregulated
Downregulated
O
DEGs involved in Migration
4
3
2
1
14
20
Positive regulation of migration
5
2
Epithelial to Mesenchymal transition
3
4
Mesenchymal migration
3
18
Cellular Matrix and Adhesion molecules
0
5
10
15
20
25
Downregulated
Upregulated
P
Vulcano Plot - Cell motility
-log10 (adjusted p-value)
60
20
0
Kif20b
Aire
Aspm
Depc1b
Fbxo5
Anln
Akap12
Wdr62
Thbs1
Spdl1
Vash1
Tnfaip6
Pla2g3
Catsper2
Apc2
Ackr3
Apq1
P2ry6
Cdh1
Plxna4
Alox5
Apob
Myh10
Dnah9
Smpd3
-3
0
6
log2 Fold Change

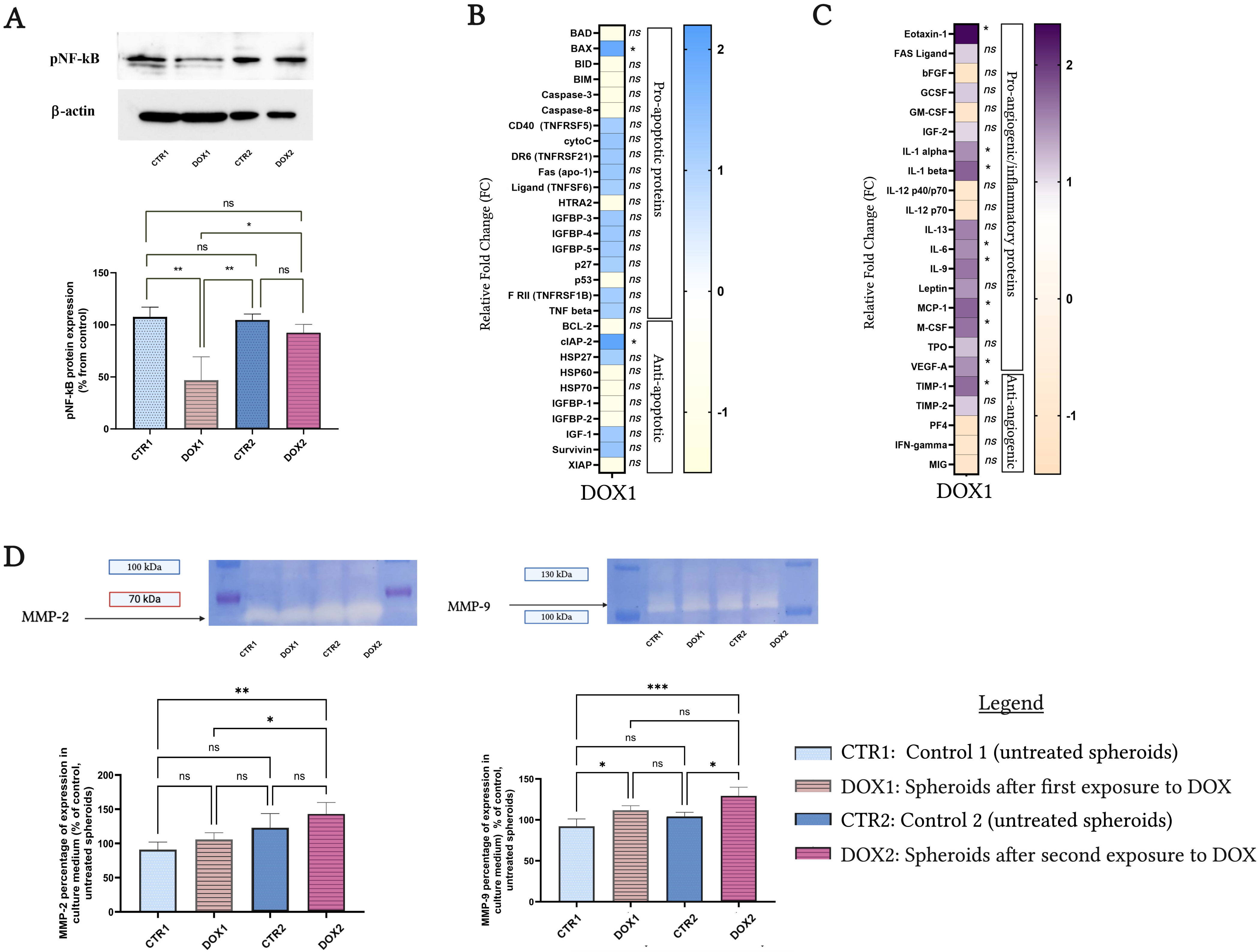
A
pNF-kB
β-actin
CTR1
DOX1
CTR2
DOX2
pNF-kB protein expression (% from control)
0
50
100
150
ns
*
ns
**
**
ns
B
Relative Fold Change (FC)
BAD
BAX
BID
BIM
Caspase-3
Caspase-8
CD40 (TNFRSF5)
cytoC
DR6 (TNFRSF21)
Fas (apo-1)
Ligand (TNFSF6)
HTRA2
IGFBP-3
IGFBP-4
IGFBP-5
p27
p53
F RII (TNFRSF1B)
TNF beta
BCL-2
cIAP-2
HSP27
HSP60
HSP70
IGFBP-1
IGFBP-2
IGF-1
Survivin
XIAP
Pro-apoptotic proteins
Anti-apoptotic
2
1
0
-1
DOX1
C
Relative Fold Change (FC)
Eotaxin-1
FAS Ligand
bFGF
GCSF
GM-CSF
IGF-2
IL-1 alpha
IL-1 beta
IL-12 p40/p70
IL-12 p70
IL-13
IL-6
IL-9
Leptin
MCP-1
M-CSF
TPO
VEGF-A
TIMP-1
TIMP-2
PF4
IFN-gamma
MIG
Pro-angiogenic/inflammatory proteins
Anti-angiogenic
2
1
0
-1
DOX1
D
100 kDa
70 kDa
MMP-2
130 kDa
100 kDa
MMP-9
MMP-2 percentage of expression in culture medium (% of control, untreated spheroids)
0
50
100
150
200
**
*
ns
ns
ns
ns
MMP-9 percentage of expression in culture medium) % of control, untreated spheroids)
0
50
100
150
***
ns
ns
*
ns
*
Legend
CTR1: Control 1 (untreated spheroids)
DOX1: Spheroids after first exposure to DOX
CTR2: Control 2 (untreated spheroids)
DOX2: Spheroids after second exposure to DOX

Table 1. Angiogenesis results

	Protein	Fold change (FC) of inhibition (-) and stimulation (+) of proteins in spheroids after first exposure to DOX
Pro-angiogenic/inflammatory	Eotaxin-1	2.3085±0.8410 (****)
	Fas Ligand	1.0995±0.3108 (ns)
	bF-GF	0.8277±0.2533 (ns)
	GCSF	1.1306±0.4009 (ns)
	GM-CSF	0.8620±0.1365 (ns)
	IGF-2	1.0509±0.0482 (ns)
	IL-1α	1.4897±0.0113 (*)
	IL-1 β	1.7684±0.3061 (**)
	IL-12 p40/p70	0.9880±0.0696 (ns)
	IL-12 p70	0.8363±0.1300 (ns)
	IL-13	1.5612±0.0682 (*)
	IL-6	1.4972±0.6348 (*)
	IL-9	1.6400±0.6093 (**)
	Leptin	1.4493±0.2680 (ns)
	MCP-1	1.7386±0.1386 (**)
	M-CSF	1.6628±0.1408 (**)
	TPO	1.1907±0.1472 (ns)
	VEGF-A	1.4714±0.0397 (*)
Anti-angiogenic/ inflammatory	TIMP-1	1.7002±0.0444 (**)
	TIMP-2	1.1253±0.1171 (ns)
	PF4	0.7706±0.0852 (ns)
	IFN-γ	0.9155±0.0053 (ns)
	MIG	0.8775±0.0095 (ns)

	Protein	Fold change (FC) of inhibition (-) and stimulation (+) of proteins in spheroids after first exposure to DOX
Pro-apoptotic	BAD	0.8719±0.2587 (ns)
	BAX	3.9098±0.1818 (*)
	BID	1.7546±0.2080 (ns)
	BIM	1.6089±0.0877 (ns)
	Caspase-3	1.6421±0.3527 (ns)
	Caspase-8	0.8086±0.0087 (ns)
	CD40 (TNFRSF5)	2.3207±1.1964 (ns)
	cytoC	2.6378±0.0353 (ns)
	DR6 (TNFRSF21)	2.5238±0.3125 (ns)
	Fas (apo-1)	2.5883±0.0290 (ns)
	Fas Ligand (TNFSF6)	2.2934±0.3596 (ns)
	HTRA2	1.7063±0.1943 (ns)
	IGFBP-3	1.2782±0.4907 (ns)
	IGFBP-4	1.2649±0.5796 (ns)
	IGFBP-5	1.2206±0.2061 (ns)
	p27	1.1217±0.2385 (ns)
	p53	0.9119±0.5996 (ns)
	TNF RII (TNFSF1B)	1.1745±2.3490 (ns)
	TNF b	1.4982±2.9964 (ns)
Anti-apoptotic	BCL-2	1.9620±0.1855 (ns)
	cIAP-2	4.1014±1.1240 (*)
	HSP27	2.3136±0.2804 (ns)
	HSP60	1.6628±0.4102 (ns)

Table 2. Apoptosis results

Efflux pump
Drug
Metabolizing enzymes
Metabolites
Cytoplasm
G1
S
G2
M
STOP
Cancer cell apoptosis
EMT transition

Mechanisms of early diagnosis of DOX resistance

Drug inactivation and efflux

↓ *TOP2A*

Alteration of cell cycle

↓ *CDK1*
Mad2l1
Ticrr
Cdc20
Bub1

Inhibited Apoptosis

↓ *Sfn*
Cyclin G1

↑ Bax
cIAP2

DNA damage and repair response

↓ *BRIP1*
BARD1
Rad51
Rmi2

Aggressiveness phenotype

↑ Angiogenesis

↑ VEGF
Ackr3
Aqp1

Invasion and metastasis potential

↑ MMP-2
MMP-9
MMP-15

↑ Secretion of:

- ○ Chemokines
- ○ Cytokines
- ○ Interleukins
- ○ MMPs